Article

Bioinspired *Stevia rebaudiana* Green Zinc Oxide Nanoparticles for the Adsorptive Removal of Antibiotics from Water

Hania A. Guirguis, Noha Youssef, Mariam William, Dania Abdel-Dayem, and Mayyada M.H. El-Sayed*

Read Online

ACCESS | Metrics & More | Article Recommendations | SI Supporting Information

ABSTRACT: Green zinc oxide nanoparticles (ZnO NPs) synthesized using *Stevia rebaudiana* as a reducing agent were investigated as ecofriendly adsorbents for the removal of the antibiotics ciprofloxacin (CIP) and tetracycline (TET) from water. Green ZnO NPs were synthesized using a rapid novel approach that did not require annealing or calcination at high temperatures to produce mesoporous NPs with a size range of 37.36−71.33 nm, a specific surface area of 15.28 m^2/g, and a negative surface charge of −15 mV at pH 5. The green ZnO NPs exhibited an antioxidant activity of 85.57% at 250 μg/mL and an antibacterial activity with MIC and MBC of 50 and 100 mg/mL, respectively, against both *Escherichia coli* and *Staphylococcus aureus*. The best adsorption performance was achieved using a 4 g/L dose and pH 5, yielding, respectively, 86.77 ± 0.82% removal and 27.07 ± 0.26 mg/g adsorption capacity for CIP at 10 mg/L and 67.86 ± 3.41% and 15.88 ± 0.37 mg/g for TET at 25 mg/L. The green ZnO NPs achieved 79.71% ± 0.28 and 61.55% ± 0.53 removal of 10 mg/L CIP and 25 mg/L TET, respectively, in a spiked tap water binary system of the two contaminants. Adsorption of CIP and TET occurred mainly via electrostatic interactions, whereby CIP was bound more strongly than TET by virtue of its charge and size. The synthesis and adsorption processes were evaluated by a stepwise regression statistical model to optimize their parameters. Lastly, the green ZnO NPs were regenerated and reused for 5 cycles, indicating their functionality as simple, reusable, and low-cost adsorbents for the removal of CIP and TET from wastewater, in accordance with SDGs #6 and 12 for the sustainable management of water.
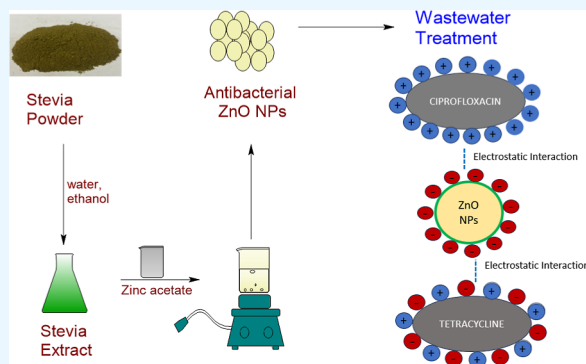
1. INTRODUCTION

As global dialogue about climate change increases, the reference to Sustainable Development Goals (SDGs) as guidance for global prosperity becomes more vital. SDG #6, which is concerned with sustainable management of water, encourages the recycling and reuse of treated wastewater.[1] Treated wastewater can be used in irrigation of edible and nonedible crops, landscapes, and other agricultural uses while playing a part in preserving the quantity and quality of the limited water resources and also contributing to SDG #2, which is related to zero hunger and can be achieved by increased agricultural output using recycled wastewater.[2,3]

One major issue with conventional wastewater treatment is the prevalence of contaminants of emerging concern (CECs) which are not completely degraded or removed during primary and secondary treatment steps.[4] The persistence of CECs and their classification have been widely researched.[4−8] Antibiotics comprise a subclass of one of the classes of CECs, which is pharmaceuticals. The continued use and reintroduction of antibiotics into the environment via reused treated wastewater leads to antimicrobial resistance and adverse effects on the ecosystem.[9] Ciprofloxacin (CIP) is a fluoroquinolone antibiotic that is prescribed to treat several infections of the bones, joints, urinary tract, and others.[10] It is not readily

biodegradable and is likely to persist in wastewater influents and effluents.[11,12] In 2018, CIP was placed on a watch list of substances for union-wide monitoring by the European Union, and its maximum detection limit was set to be 89 ng/L.[13] CIP's side effects include seizures and ruptured tendons, and it may contribute to antimicrobial resistance.[12] Out of 200 pharmaceuticals, CIP had the highest detection concentration of 6.5 mg/L in global river waters.[14] It has been detected in Mediterranean wastewater samples,[15] surface water in China with a maximum concentration of 39.22 ng/L,[16] the effluent of European wastewater treatment plants with a maximum concentration of 316.8 ng/L,[17] in industrial wastewater in India with a maximum concentration of 28−30 mg/L,[18] and in surface and wastewater in the USA with a maximum concentration of 1292 ng/L.[19] The second antibiotic pertinent to this study is tetracycline (TET) which is also poorly
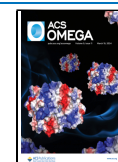
biodegradable and prescribed to treat infectious diseases in humans and to promote animal growth.[20,21] It is the second most produced and consumed antibiotic in the world as it is used to promote livestock growth, which explains the prevalence of its resistant genes.[21,22] In addition to antimicrobial resistance, TET persistence could affect the human intestine by disrupting the gut microflora.[23] TET was detected in surface and wastewater in China[12] in the $1-10$ μg/ kg range[12,24] and USA in the μg/L range,[25] and in wastewater treatment plant effluents in USA[26] and in several European countries[17] with a maximum concentration of 0.21 μg/L and 231.2 ng/L, respectively.

Several methods have been successful in the removal or degradation of antibiotic effluents, like membrane filtration,[27,28] photocatalytic degradation,[27] ozonation,[27] activated sludge,[29,30] and combinations of these treatments.[31] Adsorption has also been commonly applied for the removal of antibiotics due to its simple operation and low cost compared to the alternatives,[5] as well as the possibility of regeneration and reuse of the adsorbent.[28] CIP and TET were adsorbed by clays,[32,33] graphene,[15,34,35] and natural adsorbents.[36−39] Nanoparticles (NPs) have been explored for the adsorption of antibiotics due to their high surface area and possible surface modifications. CIP has been adsorbed by chemically synthesized Al_2O_3 NPs,[40] CuO NPs,[41] Fe_3O_4 NPs,[42] MgO NPs,[42] ZnO NPs,[38,43] and pistachio shells coated with ZnO NPs.[44] TET has also been adsorbed by nanosorbents, like chemically synthesized TiO_2 NPs,[45] sunflower husk coated with CuO NPs,[46] and pistachio shell coated with ZnO NPs.[44] Additionally, nanoparticles synthesized in a green manner, using natural resources as reducing agents, could be more environmentally friendly and suitable for adsorption due to the bioactive compounds coating them.[9] For example, CIP has been adsorbed by nanosilica synthesized from rice husk[47] and iron-based magnetic carbon nanocomposites that were prepared from mango biomass.[48] TET has also been adsorbed by green nanosorbents like Fe/ZnO chitosan composite beads.[49]

In this work, *Stevia rebaudiana* is used as a reducing agent to synthesize green ZnO NPs for the adsorption of CIP and TET in water. *S. rebaudiana* is a known sugar substitute that exhibits multiple biological activities[50,51] due to being a rich source of reducing sugars and phenolic compounds.[52] It has been used to synthesize AgNPs,[53,54] AuNPs,[55] and ZnS NPs.[56] It was also used to synthesize ZnO NPs; however, the synthesis process required a high annealing temperature of 600 °C.[57] The synthesis method applied in this work is simple, rapid, reproducible, does not require high annealing temperatures or harsh chemical consumption, and utilizes a natural reducing and capping agent for the ZnO NPs, thus alleviating the concern of nanoparticle presence in water.[9] In addition to the new approach in synthesizing the green ZnO NPs, the value of this work lies in the novelty of their use as adsorbents for CIP and TET in a comprehensive study that evaluates the effect of adsorption parameters, applies kinetic and isotherm modeling, explores regeneration and reuse of the adsorbent, investigates the behavior in a binary system, and utilizes factorial design to optimize adsorption and synthesis parameters.

2. MATERIALS AND METHODS

2.1. Materials. For the synthesis of the green ZnO NPs, *S. rebaudiana* ground leaves were obtained from and identified by the herbarium of the American University in Cairo, ethanol

(96% v/v) was purchased from Piochem Co. (Giza, Egypt). Visking dialysis tubes with pore diameters of ca. 25 Å were purchased from Serva (Heidelberg, Germany), zinc acetate dihydrate was purchased from Loba Chemie PVT. Ltd. (Mumbai, India), and sodium hydroxide pellets were purchased from Sigma-Aldrich (Germany). For the sake of comparison of adsorption behavior, commercial ZnO NPs, with an average size of 350 nm, were purchased from Nawah Scientific (Cairo, Egypt).

For chemical and biological analysis, phenol (5%) from BDH Chemicals (England) and sulfuric acid (98% v/v) from Penta (Prague, Czech Republic) were obtained for the determination of carbohydrate content. For the determination of phenolic content, gallic acid (>99%) was purchased from Roth Chemicals (Karslruhe, Germany), Folin-Ciocalteu's Phenol reagent was bought from Loba Chemie PVT. Ltd. (Mumbai, India), while sodium carbonate anhydrous (extra pure grade) was purchased from TopChem (Giza, Egypt). For the determination of the DPPH antioxidant assay, 1,1-diphenyl-2-picryl-hydrazyl (DDPH) was purchased from Sigma-Aldrich (USA) and methanol (99.8%) was purchased from Research-Lab Fine Chem Industries (Mumbai, India).

For the adsorption experiments, ciprofloxacin (purity grade: 99%) hydrochloride was supplied by the Egyptian International Pharmaceutical Industries Co. (EIPICo, Cairo, Egypt), and tetracycline (purity grade: 97.5%) was also supplied in kind by Intervet Egypt for Animal Health (Cairo, Egypt).

2.2. Synthesis of Green ZnO NPs. The *S. rebaudiana* extract was prepared using ultrasound-assisted extraction followed by ethanol evaporation; the extraction method is similar to that reported in our previous work on mangrove extract.[58] For the synthesis of the green ZnO NPs, 0.1 M zinc acetate solution in 100 mL of deionized water was heated until around 35 °C while stirring at 500 rpm, and then the *S. rebaudiana* extract solution (1 or 2 g/L) was added dropwise in a ratio of 5:2 or 5:3 v/v (zinc acetate solution/extract solution). A 4 M NaOH solution was added dropwise to the mixture until the pH value reached 10. Heating continued until the mixture reached 70 °C, after which it was left at constant temperature under stirring at 500 rpm for 2 or 3 h. The magnet sizes used for stirring were 2.5 or 4 cm in diameter. Afterward, the mixture was centrifuged, and the supernatant was discarded. The precipitate was washed and centrifuged twice to remove impurities, then left to dry at room temperature. The dry green ZnO NPs were ground into fine powder for characterization and further use.

2.3. Characterization. Synthesis of green ZnO NPs was confirmed through UV−visible spectroscopy (Varian Cary 500 Scan, California, USA), and the band gap was calculated using eq 1, where E_{bg} is the band gap energy in joules, h is Planck's constant (6.626×10^{-34} m^2 kg/s), c is the speed of light (3×10^8 m/s), and λ is the absorbance wavelength. The energy value is then converted from joules to eV.[59] The chemical structures of the *S. rebaudiana* extract and green and commercial ZnO NPs were analyzed by Fourier transform infrared spectroscopy (FTIR) (TGA/FT-IR Thermo Fisher Scientific Nicolet 380 spectrometer, Massachusetts, USA) by using the KBr method. X-ray diffraction analysis (XRD) (Bruker D8 Discover diffractometer, Massachusetts, USA) was used to identify the crystal structure and lattice planes of the green and commercial ZnO NPs. The hydrodynamic size of the green and commercial ZnO NPs used for factorial analysis and their surface charge were determined using dynamic light

scattering (DLS) and zeta potential measurements (Malvern Panalytical Zetasizer Nano Series Nano-ZS90, Malvern, UK), respectively. Shape and size of the green ZnO NPs were determined by using scanning electron microscopy (SEM) (Zeiss LEO SUPRA 55 FESEM, Oberkochen, Germany) and transmission electron microscopy (TEM) (JEOL-JEM-2100, Tokyo, Japan). For TEM, 0.01 g of green ZnO NPs were dispersed in 10 mL of distilled water and sonicated for 10 min prior to analysis. To examine the thermal degradation behavior of the green ZnO NPs, thermogravimetric analysis (TGA) was conducted (Thermo Fisher Scientific Q Series TGA Analyzer, Massachusetts, USA) using a heating rate of 10 °C/min under a nitrogen flow rate of 50 mL/min from 20 °C until 780 °C. Energy dispersive X-ray spectroscopy (EDX) measurements (NeoscopenJCM-6000 Plus, Tokyo, Japan) were used for elemental analysis of the green ZnO NPs. Lastly, Brunauer−Emmett−Teller (BET) analysis (Micrometrics ASAP 2020, Georgia, USA) was carried out to obtain the surface area and pore volume of the green ZnO NPs.

$$E_{bg} = h\frac{c}{\lambda} \qquad (1)$$

2.4. Chemical and Biological Analysis. The total carbohydrate content of the *S. rebaudiana* extract and green ZnO NPs was determined using the phenol−sulfuric acid method with minor modifications.[60] The absorbance of the phenol, sulfuric acid, and sample mixtures was measured at 490 nm (Jenway 7415 Scanning UV−vis spectrophotometer), and the total carbohydrate content was calculated using the glucose calibration curve. The total phenolic content of the *S. rebaudiana* extract and green ZnO NPs was determined via the Folin-Ciocalteu reagent assay[61] using a gallic acid calibration curve, while the absorbance was measured at 765 nm (Supporting Information, eq S1). The antioxidant activity of the *S. rebaudiana* extract and green ZnO NPs, and commercial ZnO NPs was determined for concentrations of 1000, 500, and 250 μg/mL using the DPPH radical scavenging assay with minor modification.[62] Absorbance was measured at 517 nm, and the percentage scavenging activity was calculated using ascorbic acid as a standard reference (eq S2). The antibacterial activity of the extract and green, and commercial NPs was measured against Gram-positive bacteria *Staphylococcus aureus* (ATCC 25923) and Gram-negative bacteria *Escherichia coli* (ATCC 25922). The plates were incubated for 24 h at 37 °C, after which the minimum inhibitory concentration (MIC) and minimum bactericidal concentration (MBC) were obtained. Each plate had a concentration of 4−6 × 10^5 cfu for the tested organism.

2.5. Adsorption Experiments. For each adsorption experiment, fresh stock solutions of 1000 mg/L CIP and TET were prepared and used for further dilutions. A volume of 10 mL of adsorbate−adsorbent solution was left to mix in 15 mL falcon tubes at 80 rpm on a rotary shaker and then separated and centrifuged, and the absorbance of the supernatant was measured at 274 and 275 nm for CIP and TET, respectively. Adsorption efficiency was measured by % removal (Supporting Information, eq S3) and adsorption capacity q in mg/g (Supporting Information, eq S4).

2.5.1. Effect of Parameters. For the effect of pH, antibiotic solutions were prepared at concentrations of 10 and 25 mg/L for CIP and TET, respectively, and their pH was adjusted using 0.1 M HCl or 0.01 M NaOH. The dose of green ZnO NPs used was 1 and 4 g/L for CIP and TET, respectively. The

adsorbate and adsorbent were left to mix for 4 h at 25 ± 2 °C. For the effect of adsorbent dose, 0.5, 1, 2, 3, 4, and 5 g/L of green ZnO NPs were mixed with 10 and 25 mg/L of CIP and TET, respectively, for 4 h at 25 ± 2 °C and pH 5. To measure the effect of initial concentration on adsorption, concentration ranges of 10−130 mg/L of CIP and TET were prepared and mixed with 4 g/L of the green ZnO NPs for 4 h at 25 ± 2 °C and pH 5. To examine the effect of contact time, several concentrations of CIP and TET were mixed with 4 g/L green ZnO NPs for time periods of 5, 10, 15, 20, 30, 60, 120, and 280 min at 25 ± 2 °C and pH 5. Lastly, to examine the effect of temperature on adsorption, 10 and 25 mg/L CIP and TET, respectively, were mixed with 4 g/L green ZnO NPs at pH 5 and a temperature range of 25−70 ± 2 °C.

2.5.2. Isotherm and Kinetic Modeling. To explore the interaction between the adsorbate and adsorbent, isotherm and kinetic modeling were applied. For isotherm modeling, the Langmuir and Freundlich adsorption models were applied (Supporting Information, eqs S5 and S6, respectively). To understand the kinetics of the adsorption of CIP and TET on green ZnO NPs, the pseudo-first-order, pseudo-second-order, and Elovich models were examined (eqs S7−S9, respectively).

2.5.3. Regeneration and Reuse of Adsorbent. To examine the regeneration and reuse of the adsorbent, 4 g/L green ZnO NPs were mixed with 10 and 25 mg/L CIP and TET solutions, respectively, for 4 h at 25 ± 2 °C and pH 5. After adsorption, the adsorbent was separated from the solution and washed with water and then absolute ethanol for 2 h at 60 rpm, after which it was rinsed and left to dry for reuse. This was applied for 5 cycles. The adsorptive performance of the green ZnO NPs was compared with that of commercial ZnO NPs at a dose of 4 g/L for 4 h at pH 5 and 25 ± 2 °C.

2.5.4. Binary System Adsorption Experiment. For binary system investigations, tap water and distilled water were each spiked with both CIP and TET at a concentration of 10 and 25 mg/L, respectively. To compare with the single-adsorbate system, tap water and distilled water were spiked with each antibiotic individually at the same concentration. Adsorption was conducted using 4 g/L adsorbent for 4 h at pH 5 and 25 ± 2 °C. After centrifugation to separate adsorbent and adsorbate, the absorbance of the adsorbate solution was measured using UV−vis spectrophotometry (Agilent Cary 3500 Compact UV−vis spectrophotometer, California, USA) over a range of 200−400 nm. The first derivative of the spectra was calculated, and the absorbance values were considered at 257 and 389 nm for CIP and TET, respectively.

2.6. Factorial Design for Optimization of Green ZnO NPs Synthesis and Adsorption. Four variables, including time (X), extract concentration (E), v/v ratio (R) of zinc acetate to extract, and magnet size (M), are thought to have an impact on the green ZnO NPs particle size. Two levels were assigned to each variable, with the lower and upper levels designated by −1 and 1, respectively. The variables and their levels are listed in Table 1. The dependent variable is the particle size, as measured by DLS. Factorial designs were selected to study the relationship between these four variables and the particle size of the green ZnO NPs. The factorial design was generated using R-Studio 2021.09.02 (USA).

After the experiments were run using the selected designs, regression analysis was applied to study the effect of different variables on CIP adsorption. A two-level four-factor analysis was chosen with the independent variables and their levels being time (2 and 4 h), CIP concentration (10 and 100 mg/

Table 1. Parameters and Levels Used in Factorial Design of Green ZnO NPs Synthesis, CIP Adsorption, and TET Adsorption

Green ZnO NPs Synthesis							
time (X) h		extract concentration (E) μg/L		ratio (R)		magnet size (M) cm	
−1	1	−1	1	−1	1	−1	1
2	3	1000	2000	5:2	5:3	2.5	4
CIP Adsorption							
time (X) h		concentration (C) mg/L		dose (D) g/L		temperature (T) °C	
−1	1	−1	1	−1	1	−1	1
2	4	10	100	1	4	25	70
TET Adsorption							
time (X) h		concentration (C) mg/L		dose (D) g/L			
−1	1	−1	1	−1	1		
2	4	25	100	1	4		

L), ZnO NPs dose (1 and 4 g/L), and temperature (30 and 70 °C). The four independent variables are denoted by X, C, D, and T, respectively. Similarly, for TET, a two-level, three-factorial design was chosen with the independent variables with their levels being time (2 and 4 h), TET concentration (25 and 100 mg/L), and dose (1 and 4 g/L). The three independent variables are denoted by X, C, and D, respectively. For each antibiotic, the analysis was conducted twice using the same independent variables to assess two dependent variables, which are % removal and equilibrium adsorption capacity q (mg/g). For all independent variables, the lower limit is represented by −1, while the upper limit is represented by 1. The factors, levels, and their values are listed in Table 1.

2.7. Statistical Analysis. All experiments were performed in triplicate, and the data are expressed as the mean ± standard deviation. The statistical analysis for the isotherm and kinetic modeling was conducted using linear regression analysis, while the unpaired two-tailed t-test was used for comparison studies.

3. RESULTS AND DISCUSSION

3.1. Statistical Analysis of Particle Size. To identify the significant factors and interactions that affect the particle size, a scatter plot between all pairs of variables (Figure S1a) was depicted to explore the linear relationship between the independent variables and the dependent variable.

To investigate the interaction of two factors and its effect on particle size, interaction plots (Figure S2) were constructed. All interaction plots showed an interaction between the variables.

Regression analysis was conducted, and eq 2 represents the best linear model obtained by stepwise regression analysis to describe the effects of the factors of time, concentration of extract, ratio of zinc solution to extract, and magnet sizes and their interactions on log particle size.

$$\begin{aligned} \text{Predicted log particle size} \\ = 7.2232 - 1.6952X1 - 1.5157R1 - 1.3194E1 \\ + 0.4185M1 + 2.5725X1: R1 + 1.5334X1: E1 \\ + 1.6932E1: M1 + 1.3324X1: R1: E1 - 1.5186X1 \\ : R1: E1 - 2.5212R1: E1: M1 \end{aligned} \tag{2}$$

To validate the model assumptions, Figure S1b depicts a residuals versus fits plot, which indicates that the average of errors = 0, in addition to the independence of errors and the constant variance. Figure S1c,d shows the $Q-Q$ plot and histogram for particle size residuals that are used to investigate the normality of the residuals.

The model is highly significant, with a p-value of 2.2×10^{-16} and an adjusted R^2 value of 0.9057. From eq 2, it can be noticed that the negative coefficients at their levels (−1, 1) lead to a decrease in the particle size, which is the desired
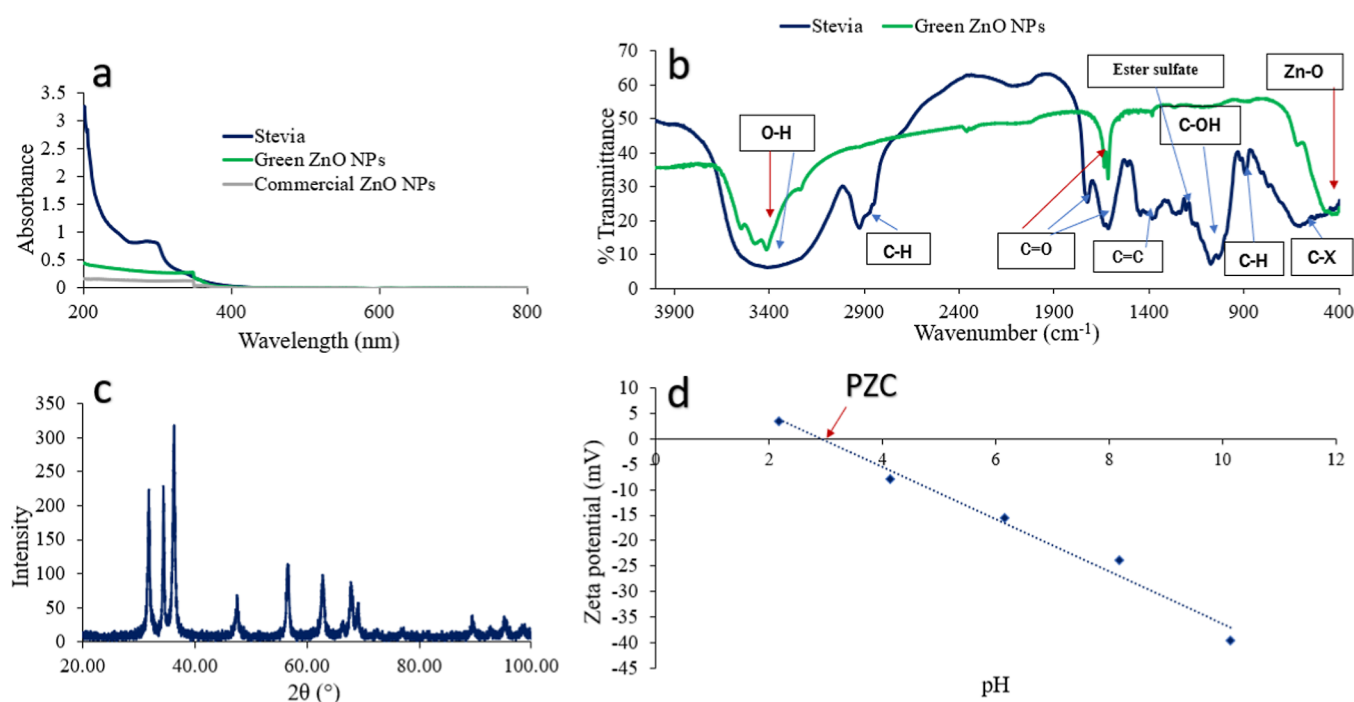
Figure 1. (a) UV−vis spectra of *S. rebaudiana*, green ZnO NPs, and commercial ZnO NPs, (b) FTIR spectra of *S. rebaudiana* and green ZnO NPs, (c) XRD spectrum, and (d) point of zero charge (PZC) of green ZnO NPs.
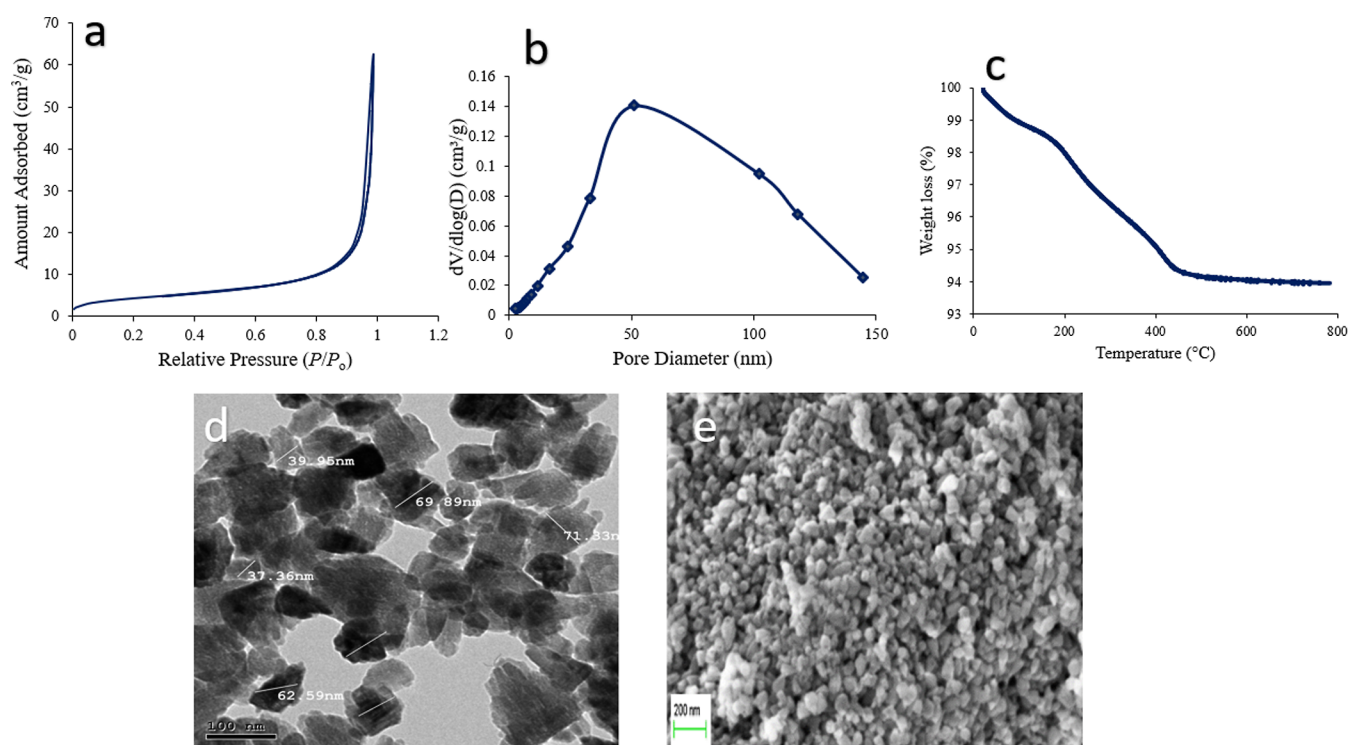
Figure 2. (a) N$_2$ adsorption−desorption on the green ZnO NPs, (b) pore size distribution of green ZnO NPs, (c) TGA profile, (d) TEM image, and (e) SEM micrograph of green ZnO NPs.

outcome. For instance, the negative coefficients of time ($X1$), ratio of zinc solution to extract ($R1$), and concentration of the extract ($E1$) at their upper levels of 1 (3 h, 5:3, and 2000 μg/L, respectively) indicate that particle size decreases, while particle size increases as magnet size goes to its upper level of 4 cm ($M1$), as inferred from the positive coefficient of magnet size. As for the two-factor interactions, they all had positive coefficients, indicating an increase in particle size. However, the interaction plots (Figure S2a) indicate that when ratio is fixed at its lower level, particle size decreases at the lower concentration level, and it also decreases when ratio and concentration are at their upper levels. The higher amount of extract contained in the upper levels of ratio and concentration indicates that as the reducing agent increases, the particle size decreases. The same can be observed for the interaction between time and magnet size, where the smallest possible particle size is obtained at the upper levels of both (Figure S2b). The larger magnet size and longer time led to faster nucleation and slowed particle growth due to capping of the green ZnO NPs by the bioactive compounds of the *S. rebaudiana* extract. For the three-factor interaction, one factor is kept constant, while the other two are varied. The positive coefficient of the interaction between X-1:$R1$:$E1$ indicates that at the lower level of time (2 h) and upper levels of ratio and extract concentration (5:3 ratio, 2000 μg/mL), the particle size increases, while it decreases when time is kept at its upper level of 3 h ($X1$:$R1$:$E1$). Lastly, the negative coefficient of $R1$:$E1$:$M1$ indicates that particle size decreases at the upper level of all three factors (5:3 ratio, 2000 μg/mL extract concentration, and 4 cm magnet). This agreed with the experimental results, and accordingly, all four factors were kept at their upper levels to obtain green ZnO NPs with the smallest possible particle size.

3.2. Characterization of NPs. The UV−vis spectra of the green-synthesized ZnO NPs and commercial ZnO NPs (Figure

1a) exhibited a maximum absorbance at 348 nm, which agrees with the ranges reported in literature.[63,64] This wavelength corresponds to a band gap energy of 3.57 eV. This is a blue shift from the value exhibited by bulk ZnO at 3.37 eV,[65] due to the smaller size of the ZnO NPs, which was around 117.01 ± 2.08 and 373.38 ± 1.18 nm for the green and commercial ZnO NPs, respectively, according to DLS measurements. The *S. rebaudiana* extract exhibits a much higher absorbance due to the myriad of bioactive compounds that it contains.

The FTIR spectrum of the *S. rebaudiana* extract (Figure 1b) displays a variety of functional groups, starting with a wide band at 3500−3400 cm^{-1}, which corresponds to the OH stretch, followed by the sp^3 C−H stretch at 3000−2800 cm^{-1}.[49,66,67] The spectrum also shows bands assigned to the C=O stretch of carboxylic acids at 1800−1600 cm^{-1},[55,59,66] a C=C alkene stretch at 1500−1300 cm^{-1},[55,63] and an ester sulfate band at 1260−1257 cm^{-1}.[68] The band at 1200−1050 cm^{-1} could correspond to the C−O stretch of alcohols, ethers, or esters and could be indicative of a glycosidic bond and/or acidic polysaccharides.[59,66,68,69] The band at 900−800 cm^{-1} corresponds to the C−H vibration of alkenes and alkynes.[55,66] Last, the band at 600−400 cm^{-1} could be attributed to O−H vibrations in phenols and alcohols or an alkyl halide bond.[55,70] The FTIR spectrum of the green ZnO NPs synthesized using the *S. rebaudiana* extract (Figure 1b) is also displayed. There is a band at 430 cm^{-1} corresponding to the Zn−O stretch,[59,63] followed by two bands at 1800−1600 and 3500−3400 cm^{-1} that correspond to the carbonyl and hydroxyl stretches, respectively.[59,63] The presence of the latter two groups could be due to the metabolites of the *S. rebaudiana* extract, which coat the green ZnO NPs. The decrease in the intensity of some bands and the distortion of their shape relative to the bands of the *S. rebaudiana* extract could be attributed to the involvement of the corresponding functional groups in the

synthesis process,[54] and the absence of other bands could be attributed to the participation of their corresponding functional groups in the reduction of Zn^{2+} to Zn and the ensuing formation of green ZnO NPs. The FTIR spectrum of the commercial ZnO NPs (Figure S3a) indicates the presence of O−H, C═O, and Zn−O functional groups, as was shown in the spectrum of the green nanoparticles, but the peaks appear with greater intensities and no distortions.

The XRD spectrum of the green ZnO NPs (Figure 1c) displays three major 2θ peaks at 31.68, 34.31, and 36.22°, corresponding to lattice planes (100), (002), and (101), respectively. The minor peaks at 47.49, 56.50, 62.81, and 67.84° correspond to lattice planes (102), (110), (103), and (200), respectively. This pattern is characteristic of the ZnO NPs XRD spectrum, corresponding to a hexagonal wurtzite structure.[57,71] The commercial ZnO NPs XRD spectrum (Figure S3b) similarly displays the same characteristic pattern with three major 2θ peaks at 31.82, 34.49, and 36.23°, corresponding to lattice planes (100), (002), and (101), respectively. The minor peaks at 47.63, 56.57, 62.99, and 68.15° correspond to lattice planes (102), (110), (103), and (200), respectively.[72] The green ZnO NPs have a negative surface charge at alkaline pH values reaching −40 mV at pH 10, while they have a slightly positive to neutral surface charge at highly acidic pH values, as per the zeta potential graph (Figure 1d). The zeta potential of the commercial particles was found to be −15 mV at pH 5, which is similar to the zeta potential of the green ZnO NPs at the same pH value.

As for the textural properties of the ZnO NPs, the BET isotherm (Figure 2a), which pertains to the N_2 adsorption−desorption on the green ZnO NPs, indicates a type IV isotherm with a small hysteresis loop, corresponding to mesopores with a pore size range of 2−50 nm. The type IV isotherm suggests strong interactions between adsorbent and adsorbate and monolayer coverage followed by multilayer adsorption.[57,73] The BET and Langmuir surface areas were measured to be 15.28 and 22.62 m^2/g, respectively. The pore size distribution (Figure 2b) confirms the presence of mostly mesopores, along with some macropores. The pore volume and pore width were estimated to be 0.095 cm^3/g and 30.13 nm, respectively, according to the Barrett−Joyner−Halenda (BJH) model using the desorption curve. Thermal stability of the green ZnO NPs was studied by TGA analysis, and the thermogram (Figure 2c) displays a sample weight loss of about 6.05%, which can be attributed to moisture loss up until 100 °C followed by possible thermal degradation of the metabolites involved in the synthesis process. The temperature increment did not lead to significant weight loss, indicating the thermal stability of the green ZnO NPs.[57]

For the morphological properties of the green ZnO NPs, the TEM image (Figure 2d) confirms that the particles are of the nanoscale with a wide size range of 37.36−71.33 nm, which is lower than the average hydrodynamic size obtained through DLS measurements (117.01 ± 2.08 nm) due to the presence of the hydrated layer. SEM imaging (Figure 2e) depicts the green ZnO NPs to have a nonuniform spherical shape, which agrees with the finding of Khatami et al., who synthesized ZnO NPs using S. rebaudiana extract.[57] EDX analysis (Figure S4a) identifies the elemental composition of the green ZnO NPs, indicating strong Zn and O signals followed by a weak C signal that could stem from the S. rebaudiana metabolites.[57,74] Nitrogen was not detected, which agrees with the FTIR spectrum that lacked an amine peak. Traces of chlorine and

sulfur were detected, which could be corroborated by the presence of the alkyl halide group and ester sulfate band at 600−400 and 1260−1257 cm^{-1}, respectively, in the FTIR spectrum.

3.3. Chemical and Biological Analysis. The carbohydrate content (Figure 3a) of S. rebaudiana is 75.25% ± 1.24,
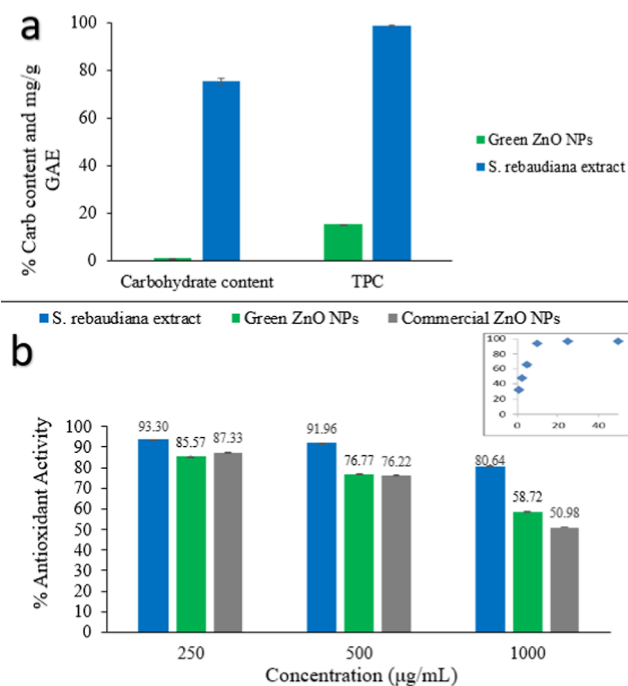
Figure 3. (a) Chemical analysis and (b) antioxidant activity of S. rebaudiana, green ZnO NPs, and commercial ZnO NPs. Values are expressed as mean ± SD (n = 3). Inset of (b) is % DPPH scavenging activity for ascorbic acid.

while that of the green ZnO NPs is 1.04% ± 0.07, which could be owed to the compounds capping the green ZnO NPs.[68] However, the content is significantly lower than that in S. rebaudiana, probably due to the consumption of a portion of the carbohydrates during the reduction process. The small percentage of carbohydrates could be attributed to the compounds capping the green ZnO NPs. The same trend is observed for the total phenolic content (TPC), which is 98.78 ± 0.0015 and 15.4 ± 0.0006 mg/g GA for S. rebaudiana extract and green ZnO NPs, respectively[75,76]

The antioxidant activity (Figure 3b) of the S. rebaudiana extract, green ZnO NPs, and commercial ZnO NPs was measured for three concentrations of each species. The extract exhibits the highest antioxidant activity due to its unbound metabolites and high phenolic and carbohydrate contents, while green ZnO NPs exhibit a significantly higher scavenging activity (P < 0.05) than the commercial ones at the highest concentration of 1000 μg/mL, while they show a significantly lower IC_{50} value (P < 0.05) (Table 2), indicating their higher antioxidant effect. There is a general trend of decrease in the antioxidant activity with increasing concentration. ZnO NPs decrease oxidative stress by reduction or radical scavenging due to the electron donation potential of the oxygen group in ZnO.[72,77]

The antibacterial activities (Table 2) of S. rebaudiana, green ZnO NPs, and commercial ZnO NPs against Gram-positive S. aureus are all the same. In addition, the MBC of the green ZnO

Table 2. Antioxidant Activity (IC$_{50}$) and Antibacterial Activity of *S. rebaudiana*, Green ZnO NPs, and Commercial ZnO NPs

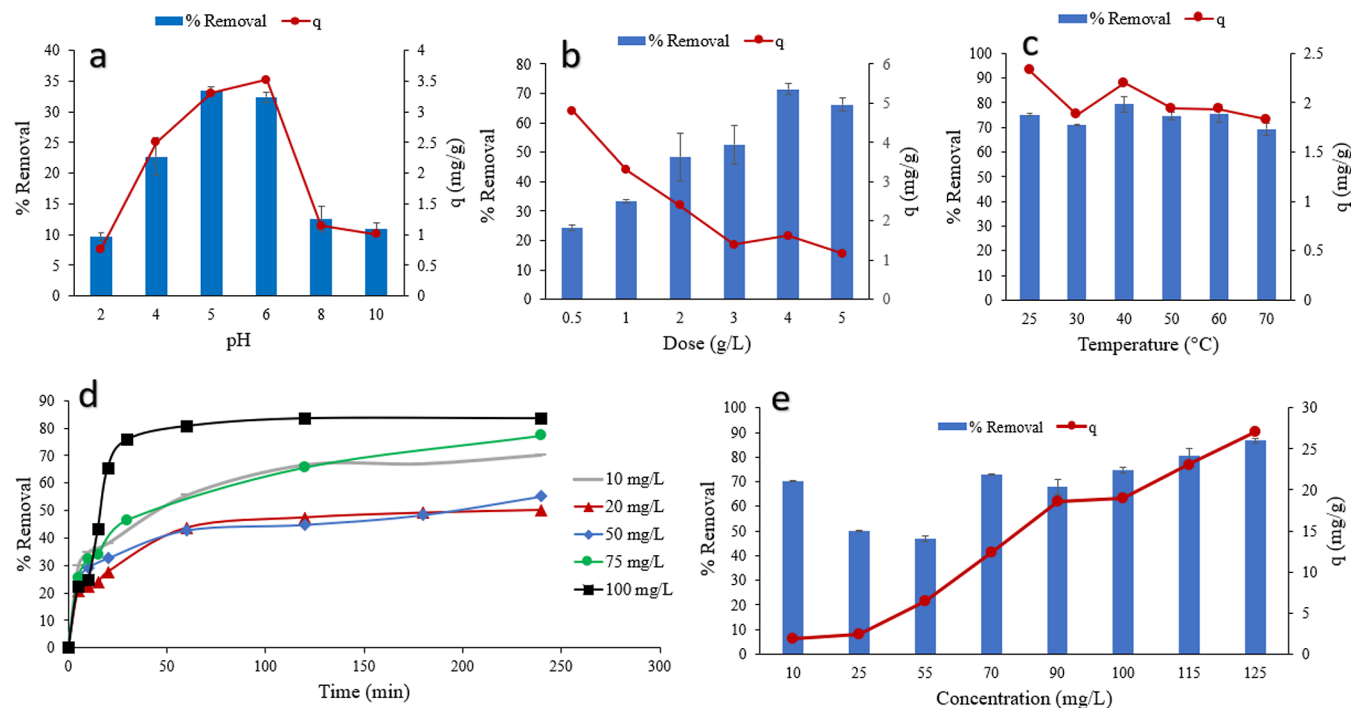|	antioxidant activity	E. coli (gram-negative)		S. aureus (gram-positive)	
	IC$_{50}$ (μg/mL)	MIC (mg/mL)	MBC (mg/mL)	MIC (mg/mL)	MBC (mg/mL)
S. rebaudiana extract	98.62	25	100	50	100
green ZnO NPs	92.80	50	100	50	100
commercial ZnO NPs	97.54	25	50	50	100

Figure 4. Effect of (a) pH, (b) dose, (c) temperature, (d) time, and (e) initial concentration on CIP adsorption by green ZnO NPs.

NPs against Gram-negative *E. coli* is the same as that of *S. rebaudiana* extract. The values are comparable to the highest antibacterial activity reported against *E. coli* and *S. aureus* by ZnO NPs, which were chemically synthesized using sol−gel and hydrothermal methods.[78] These results indicate that green ZnO NPs could be used in water disinfection, in addition to their adsorption applications. The antibacterial mechanism of the ZnO NPs involves releasing zinc ions into the cell to inhibit the electron transport chain by generating reactive oxygen species which can inhibit cell functions.[79]

3.4. Adsorption Performance. *3.4.1. CIP Adsorption.* The effects of different parameters on CIP adsorption are examined. For the effect of pH (Figure 4a), both *q* and percentage removal increase with increasing pH until pH 5−6, after which they decline. Below this pH range, CIP has a net positive charge, as per its speciation diagram (Figure S5), while the green ZnO NPs possess a net negative surface charge (Figure 1d), which results in possible electrostatic binding between CIP and the green ZnO NPs. The highest percentage removal and adsorption capacity values were 33.46 ± 0.52% and 3.3 ± 0.1 mg/g, respectively, at pH 5 and conditions of 10 mg/L initial concentration, 1 g/L dose, 4 h contact time, and 25 ± 2 °C. As such, pH 5 was chosen as the working pH for CIP adsorption experiments since it is the natural pH of deionized water and does not require the use of harsh chemicals for adjustments. The pH range of 4−6 was also chosen in several previous studies on CIP adsorption.[39,41,42,80]

For the effect of adsorbent dose (Figure 4b), % removal increases with increasing dose from 0.5 to 4 g/L due to an increase in active sites, while *q* decreases, possibly due to the implied decrease in mass transfer of the adsorbate as the amount of adsorbent increases.[81] The highest % removal of 71.49 ± 1.72% is achieved using 4 g/L green ZnO NPs, 10 mg/L CIP, pH 5, and 4 h of contact time at 25 ± 2 °C. Temperature is observed to have no prominent effect on CIP adsorption (Figure 4c), similar to a previously reported study on CIP adsorption by Mohammed et al. in 2020.[44] Thus, 25 °C is chosen as the working temperature at which the % removal is 75.17 ± 0.36%. The time profiles for CIP adsorption are studied at 5 initial concentrations up until 4 h to ensure equilibrium (Figure 4d). Adsorption occurs rapidly in the first half hour of operation and then reaches equilibrium after 60−120 min. This time range is in agreement with previous CIP adsorption studies.[39,41,44] Last, the effect of initial concentration on CIP adsorption (Figure 4e) reveals an increase in *q* with an increase in the initial concentration due to the improved mass transfer resulting from increasing the concentration gradient between the bulk of the solution and the adsorbent surface.[44,81] The highest *q* value and % removal are recorded to be 27.07 ± 0.26 mg/g and 86.77 ± 0.82%, respectively, at 125 mg/L initial CIP concentration.

Stepwise regression analysis was applied to study the relationship between the independent variables of time, dose, concentration, and temperature and the CIP adsorption efficiency-dependent variables. First, the scatter plots (Figure
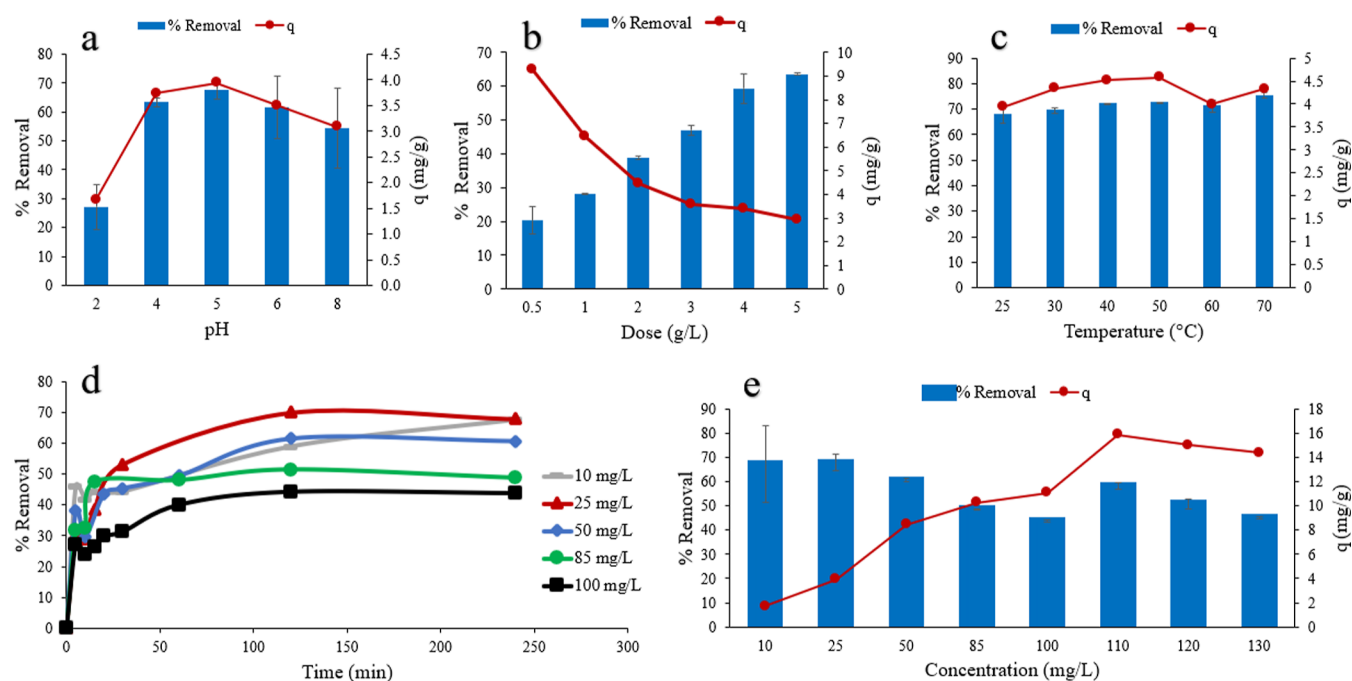
Figure 5. Effect of (a) pH, (b) dose, (c) temperature, (d) time, and (e) concentration on TET adsorption by green ZnO NPs.

S7) between all pairs of variables indicate that there is no relationship between the independent variables; however, they influence the dependent variables log q and log % removal. Residuals versus fits plots, Q−Q plots, and histograms were constructed for log q and log % removal (Figure S8). Interaction plots of the different variables were also constructed to display the effect of different combinations of the different levels of all factors on the mean of log q and log % removal (Figure S9).

Equation 3 represents the linear model that best predicts q. The equation describes the effect of the different variables and their interactions on log q. The model is highly significant, with a p-value of 2.2×10^{-16} and an adjusted R^2 of 0.9938. Three main coefficients and coefficients of seven interactions were found to be significant with p-values < 0.05. The positive coefficient of $C1$ indicates that log q increases at the upper concentration level (100 mg/L) due to increasing the mass-transfer driving force. The negative coefficient of $D1$ indicates that log q decreases at the upper dose level (4 g/L) due to particle agglomeration, whereas the positive coefficient of $T1$ indicates that the temperature, on its own when applied at the upper level (70 °C), leads to an increase in log q. However, the negative coefficient of $C1{:}T1$ indicates that log q decreases at upper levels of both temperature and concentration, as observed experimentally. Time on its own was not found to be a significant parameter in this analysis. The positive coefficients of $X1{:}C1$ and $C1{:}D1$ indicate that increasing concentration while having time and dose at their higher levels also increases log q. The positive coefficient of $X1{:}D1{:}C1{:}T1$ indicates that adsorption capacity increases at higher levels of all of the factors due to their interaction together.

$$\text{Predicted log } q = 1.17778 + 2.26788C1 - 0.623D1$$
$$+ 0.13413T1 + 0.53833X1{:}C1$$
$$+ 0.32922C1{:}D1 - 0.52663C1{:}T1$$
$$- 0.59231X1{:}C1{:}D1 - 0.76396X1{:}C1$$
$$: T1 - 0.24099C1{:}D1{:}T1$$
$$+ 0.73985X1{:}C1{:}D1{:}T1 \quad (3)$$

Equation 4 represents the linear model used to predict log % removal. The model is highly significant with a p-value of 2.2×10^{-16} and an adjusted R^2 of 0.9685. The positive coefficient of $D1$ indicates that log % removal increases at the upper dose level (4 g/L) due to the increase in the available adsorption sites. The positive $T1$ coefficient indicates that removal increases at the upper temperature levels, but, similar to the log q equation, the interaction of $C1{:}T1$ indicates that the upper levels of concentration and temperature decrease log % removal. The interaction of the upper concentration level with either the upper level of dose or time leads to an increase in log % removal. The positive coefficient of the last interaction $X1{:}C1{:}D1{:}T1$ indicates that log % removal increases at the upper levels of all of the factors due to their interactions together. Concentration and time were not found to significantly (p-value > 0.05) affect log % removal on their own.

$$\text{Predicted log \% removal}$$
$$= 3.397124 + 0.803082D1 + 0.243472T1$$
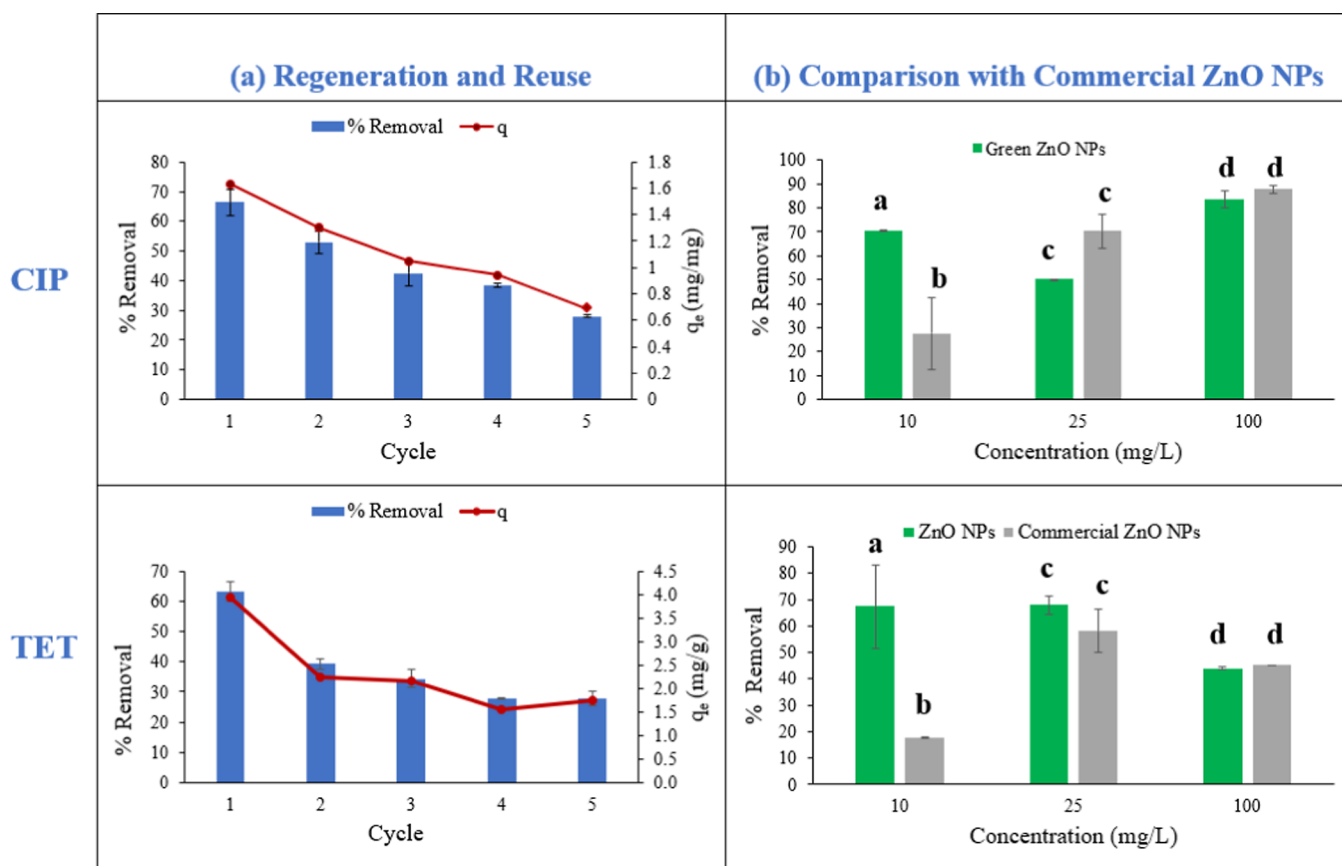$$+ 0.537678X1{:}C1 + 0.306120C1{:}D1$$
$$- 0.636242C1{:}T1 - 0.180646D1{:}T1$$
$$- 0.590068X1{:}C1{:}D1 - 0.763295X1{:}C1{:}T1$$
$$- 0.217931C1{:}D1{:}T1 + 0.819324X1{:}C1{:}D1{:}T1$$
$$\quad (4)$$

Figure 6. (a) Regeneration and reuse of green ZnO NPs after CIP and TET adsorption and (b) comparison of their adsorptive performance with commercial ZnO NPs. Groups with the same letters have insignificantly different values ($p > 0.05$).

3.4.2. TET Adsorption. Using the same reasoning adopted in CIP adsorption, we investigated TET adsorption under different conditions. From Figure 5a, pH 5 was selected as the optimum pH since it yields the highest % removal and q values of $67.86 \pm 3.41\%$ and 3.94 ± 0.20 mg/g, respectively, for 25 mg/L TET, 4 g/L ZnO NPs, 4 h contact time, and 25 ± 2 °C. This could be ascribed to the electrostatic interaction between the zwitterionic TET at pH 5 (Figure S6) and the negatively charged green ZnO NPs (Figure 1d). This pH lies within the pH range of 5−6 deployed in previous TET adsorption studies.[35,46,82]

For the effect of adsorbent dose (Figure 5b), similar to CIP adsorption, % removal increases with increasing the dose from 0.5 to 5 g/L due to an increase in active sites, while q decreases due to aggregation of particles. The same trend was observed for other TET adsorbents like pumice stone and natural Iraqi bentonite clay.[83,84] The highest % removal of $63.59 \pm 0.29\%$ is observed for the 5 g/L dose, 25 mg/L initial concentration, pH 5, and 4 h of contact time at 25 ± 2 °C. The 4 g/L dose removes $59.27 \pm 4.46\%$ of TET, which is comparable to the removal obtained by the 5 g/L dose. Hence, 4 g/L is chosen as the optimum adsorbent dose, which is the same dose chosen for the CIP experiments. Similar to CIP adsorption, temperature does not have a considerable effect on TET adsorption (Figure 5c), and this trend was also reported in other TET adsorption studies.[44] The working temperature of 25 °C shows a % removal of $67.86 \pm 3.41\%$. The time profiles for TET adsorption (Figure 5d) demonstrate rapid adsorption in the first 30 min, as in the case of CIP adsorption, and then they reach equilibrium after about 120 min. This time range is in

agreement with several TET adsorption studies.[82−85] Last, the effect of initial concentration on TET adsorption (Figure 5e) over a range of concentrations of 10−130 mg/L reveals that % removal decreases with increasing initial concentration due to the saturation of adsorption sites at higher concentrations. The highest % removal of $67.86 \pm 3.41\%$ is attained at 25 mg/L TET. The adsorption capacity, however, increases with increasing the initial concentration due to the mass-transfer effect, as was the case with CIP adsorption. The highest q of 15.88 ± 0.37 mg/g is obtained at 110 mg/L TET.

Stepwise regression analysis was again applied to study the effect of the four independent variables on the TET adsorption efficiency. The scatter plots (Figure S10) reveal that there is no linear relationship between the independent variables; however, they are linearly related with the dependent variables q and % removal. Residuals versus fits plots, $Q−Q$ plots, and histograms were constructed for log q and log % removal (Figure S11). The interaction plots manifested the effect of the different factors on one another at their different levels and their effect on the mean of log q and log % removal (Figure S12).

Equation 5 represents the linear model deployed for predicting the log q. The model is highly significant, with a p-value of 2.2×10^{-16} and an adjusted R^2 of 0.9579. The positive $C1$ coefficient indicates that log q increases at the upper TET initial concentration (100 mg/L) due to mass-transfer effects. The negative $D1$ coefficient indicates that log q decreases at the upper dose level (4 g/L) since adsorption capacity decreases with increasing adsorbent dose. At the upper time level (4 h), log q is predicted to increase, as per the
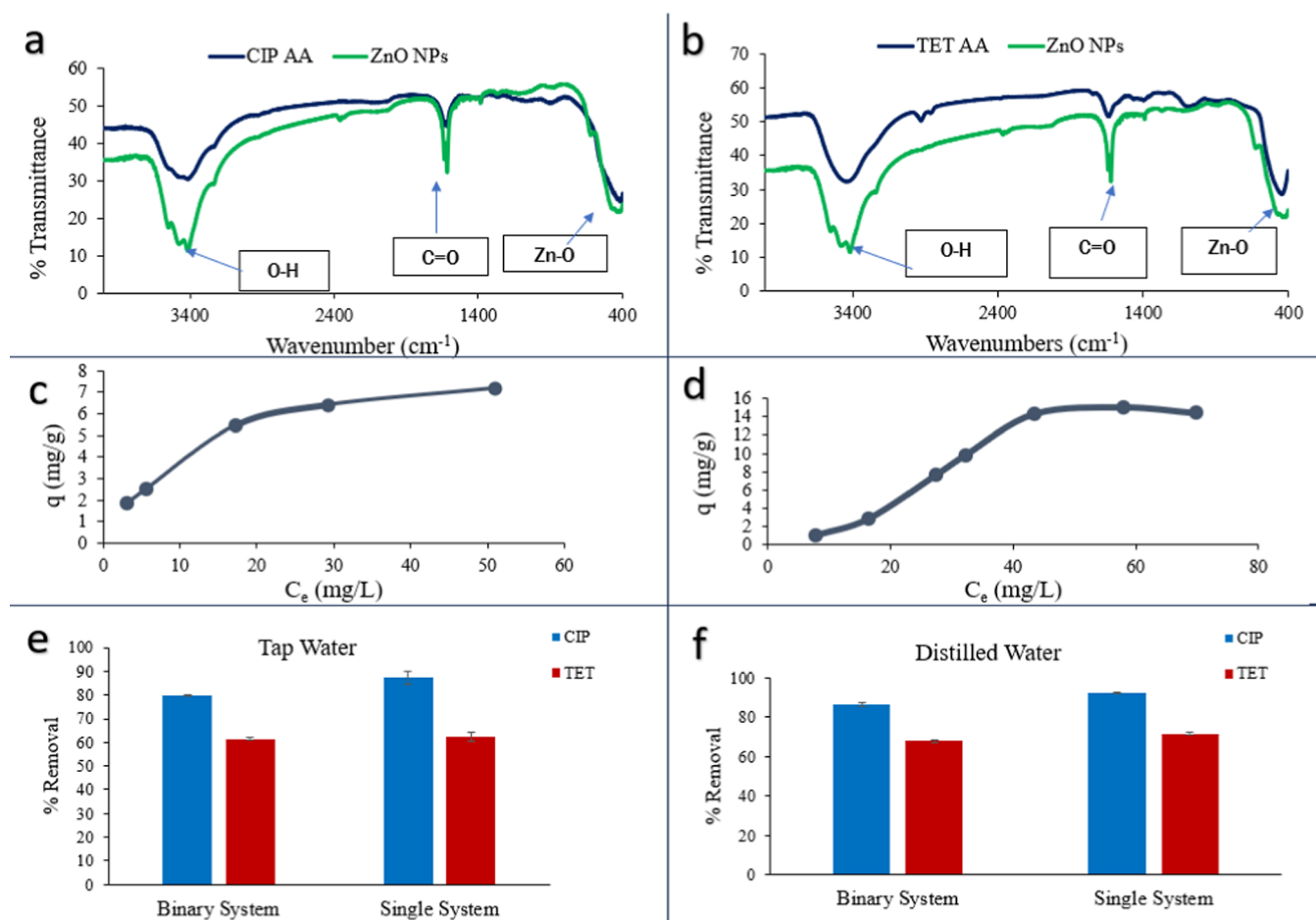
Figure 7. FTIR spectra of green ZnO NPs before (green lower curve) and after adsorption (blue upper curve) of (a) CIP and (b) TET. Adsorption isotherms of (c) CIP and (d) TET. % Removal of CIP and TET in binary and single systems in (e) tap water and (f) distilled water.

positive $X1$ coefficient. To summarize, log q increases with increasing adsorbate concentration, decreasing adsorbent dose, and increasing contact time.

$$\text{Predicted log } q = 1.7422 + 1.13948C1 - 0.47265D1$$
$$+ 0.11721X1 \qquad (5)$$

For the stepwise regression conducted on log % removal, three factors were found to be significant with p-values < 0.05. Equation 6 represents the relevant linear model, which is highly significant with a p-value of 2.2×10^{-16} and an adjusted R^2 of 0.9438. The negative $C1$ coefficient indicates that log % removal decreases at the upper concentration level (100 mg/L) due to adsorption site saturation, which is consistent with the experimental results. The positive $D1$ coefficient indicates that log % removal increases at the upper adsorbent dose level (4 g/L) due to the increase in the number of adsorption sites. The positive $X1$ coefficient also indicates that log % removal increases at the upper level of time (4 h). To summarize, log % removal increases with decreasing adsorbate concentration, increasing adsorbent dose, and increasing contact time.

$$\text{Predicted log \% removal}$$
$$= 3.14403 - 0.37019C1 + 0.98176D1 + 0.13838X1 \qquad (6)$$

3.4.3. Regeneration of Green ZnO NPs. The regeneration and reuse of the green ZnO NPs are explored after CIP and TET adsorption (Figure 6a), and generally the adsorption efficiency decreases steadily over the 5 cycles of reuse until it reaches 28.04 ± 0.57 and $27.75 \pm 2.52\%$ for CIP and TET, respectively. The reuse efficiency can be improved by increasing the washing time of the green ZnO NPs between cycles; nevertheless, this experiment indicates that the green ZnO NPs can be successfully reused for the adsorption of CIP and TET. However, CIP was more difficult to desorb than TET, which implies its stronger binding to the green ZnO NPs. The % removal of CIP dropped by 13.45% in the second cycle, while that of TET decreased by about 23.68%.

3.4.4. Adsorption of Green vs Commercial ZnO NPs. The adsorptive performance of the green ZnO NPs is compared with that of commercial ZnO NPs at three concentrations for CIP and TET (Figure 6b). The green ZnO NPs display superior performance at the 10 mg/L concentration, exceeding their commercial counterparts by almost 40 and 50% for CIP and TET, respectively. At the higher concentrations of 25 and 100 mg/L, the green and commercial ZnO NPs display an insignificantly ($p > 0.05$) different performance for both CIP and TET.

3.4.5. Adsorption Mechanism. At the pH of adsorption, pH 5, the green ZnO NPs have a zeta potential of −15 mV and CIP molecules have a positive surface charge, thus suggesting an electrostatic interaction. At lower and higher pH values, adsorption efficiency decreased due to repulsion between the like charges of green ZnO NPs and CIP. Several CIP

adsorption studies point to electrostatic interaction between oppositely charged adsorbents and CIP molecules or zwitterions.[38,39,42] The same trend can be observed for the adsorption of TET by green ZnO NPs. At pH 5, when the green ZnO NPs have a zeta potential of −15 mV, TET molecules exist as zwitterions containing a positively and a negatively charged group. Below this value, both TET and the green ZnO NPs would have positive surface charges, and above it, they would have negative surface charges, leading to repulsion, as demonstrated by the effect of pH on adsorption. Several TET adsorption studies also cite electrostatic interaction between the adsorbent and TET zwitterions.[35,46,82] The green ZnO NPs are more successful in adsorbing CIP than TET, as illustrated by the higher % removal and adsorption capacity values. This could be due to the stronger electrostatic interactions between the positively charged CIP molecules and the negatively charged green ZnO NPs, while TET has a net zero charge with a positive and a negative group. The lower molecular weight of CIP (331.34 g/mol) relative to TET (444.44 g/mol) could have also facilitated its transfer and adsorption onto the pore sites. As for the specific groups responsible for adsorption, the FTIR spectra of the green ZnO NPs before and after adsorption of both CIP and TET (Figure 7a,b, respectively) indicate the distortion and decreased intensity of the carbonyl vibration and hydroxyl stretch at 1800−1600 and 3500−3400 cm^{-1}, respectively. This suggests the participation of these electron-rich groups in the adsorption of CIP and TET, which had positive surface charges and a positive group, respectively. This is further confirmed by the EDX analysis of the green ZnO NPs after the adsorption of CIP and TET (Figure S4b,c, respectively), where the intensity of the Zn, O, and C peaks is less than that displayed in the spectrum of the particles before adsorption. The participation of the carbonyl and hydroxyl groups in the adsorption of CIP and TET was previously reported.[35,46,80,86] These groups could be involved in electrostatic attraction, hydrogen bonding, and van der Waals forces.

To further explain the adsorption mechanism, isotherms are used to demonstrate the adsorption behavior of CIP and TET on green ZnO NPs. Figure 7c,d displays the adsorption isotherms for CIP and TET, respectively, for the green ZnO NPs, which demonstrate that the adsorption capacity increases with increasing equilibrium concentration. Table 3 shows that

Table 3. CIP and TET Adsorption Isotherm Modeling Parameters

Langmuir adsorption model			Freundlich adsorption model		
K_L (L/mg)	q_m (mg/g)	R^2	K_F (mg/g)(L/mg)^n	n	R^2
CIP Adsorption					
0.082	8.74	0.9851	1.066	1.93	0.9678
TET Adsorption					
0.022	25.71	0.9932	1.16	1.64	0.9387

adsorption is better explained by the Langmuir model than the Freundlich model due to its higher R^2 value, suggesting monolayer adsorption, energetically equal adsorption sites, and a lack of interaction between neighboring adsorbed molecules.[81] Several CIP and TET adsorbents have been previously fitted to the Langmuir model.[42,48,84,85] In addition, the association constants for adsorption of CIP and TET (K_L) show that the former has a higher value, indicating stronger

binding, which is consistent with the regeneration results. Figure S12 in Supporting Information depicts the CIP and TET adsorption isotherm modeling linear plots. The kinetic profiles of CIP and TET adsorption by the green ZnO NPs were fitted to the pseudo-first-order, pseudo-second-order, and Elovich models (Tables S1−S4, respectively). The kinetic linear plots for CIP and TET are shown in Supporting Information, Figure S13. Similar to most CIP and TET adsorption studies,[38,39,43,80,83−85,87] R^2 values were higher for the pseudo-second-order kinetic model, suggesting chemisorption, which can occur through the exchange of electrons between adsorbent and adsorbate. This is supported by the effect of pH, speciation of the antibiotics, and surface charge of the green ZnO NPs at the adsorption pH, which suggests electrostatic interaction.[48]

Last, Table 4 lists several CIP and TET adsorbents along with the conditions used in their adsorption studies, using % removal, q, or both as adsorption efficiency indicators. The green ZnO NPs show comparable results to those of other adsorbents, taking into account the minimal use of heat during synthesis of the adsorbent and the added benefits of antioxidant and antibacterial activities exhibited by the green ZnO NPs.

3.4.6. Adsorption in Binary System. The performance of the green ZnO NPs in real wastewater was simulated through a binary system consisting of tap water spiked simultaneously with CIP and TET at concentrations of 10 and 25 mg/L, respectively. Figure 7e displays the results of the binary system in tap water along with the single-adsorbate systems of CIP and TET for comparison. The green ZnO NPs adsorbed CIP from tap water with removal percentages of 79.71% ± 0.28 and 87.25% ± 2.69 for the binary and single systems, respectively. TET adsorption in the binary and single systems showed % removal of 61.55% ± 0.53 and 62.27% ± 1.92, respectively. Removal % is observed to be slightly higher in the single than the binary system for both CIP and TET, which can be attributed to their competition for adsorption sites on the green ZnO NPs in the case of the binary system. Figure 7f depicts binary and single system adsorption in distilled water, which shows comparable results to their tap water counterparts. The green ZnO NPs adsorbed CIP from distilled water with removal percentages of 86.2% ± 0.89 and 92.57% ± 0.19 for the binary and single systems, respectively. TET adsorption in the binary and single systems was achieved with a % removal of 67.86% ± 0.46 and 71.66% ± 0.96, respectively. Similar to the results shown for the tap water system, the single system adsorption for CIP and TET resulted in higher % removal than those achieved in the binary system. The % removal values for both CIP and TET were slightly higher in the distilled water than in the tap water system, possibly due to the interference of minerals in the adsorption process. Additionally, the % removal values for CIP in binary and single tap and distilled water systems are higher than those achieved for TET. This trend follows the explanation provided in the adsorption mechanism section, where CIP is better adsorbed by the green ZnO NPs than TET due to its stronger electrostatic interactions and its lower molecular weight.

4. CONCLUSIONS

Green ZnO NPs were successfully synthesized using the reducing sugar-rich polysaccharide extract of *S. rebaudiana* and employed in the adsorption of CIP and TET, which are widely prevalent in water and wastewater sources and have been

Table 4. Comparison with CIP and TET Adsorbents Reported in Literature

adsorbent	specific surface area (m^2/g)	pH	conc. (mg/L)	dose (g/L)	equilibrium time (min)	adsorption efficiency % removal q (mg/g)	references
			CIP				
green ZnO NPs	15.28	5	10	4	120	70.29%	this study
			125			1.84	
					60	86.77%	
						27.07	
MgO NPs	1236	6	10	1	60	85%	42
						3.46	
Fe$_3$O$_4$ NPs	140	8	100	2.5	360	24	88
CuO NPs		4	100	10	135	81.50%	41
Pistachio shell powder coated with ZnO NPs	4.24	5	60	1	60	58.15	44
			TET				
green ZnO NPs	15.28	5	25	4	120	67.86%	this study
						3.94	
sunflower husk coated with CuO NPs		6	25	1	90	18.3	46
TiO$_2$ NPs		6	10	2	1440	93.71%	45
pumice stone	11.88	3	50	10	120	74%	83
natural Iraqi bentonite clay		6−7	20	8	120	90%	84

linked to antibiotic resistance. The green ZnO NPs were synthesized in an environmentally friendly and rapid manner without the use of a chemical reducing agent or high temperatures, and yet they exhibited the same XRD spectrum as ZnO NPs synthesized using calcination at 600 °C.[57] The synthesis parameters were optimized using factorial analysis and were found to be 3 h, 4 cm magnet size, a 5:2 v/v ratio of zinc acetate solution to extract, and 2000 μg/mL of extract. The nanoparticles have a specific surface area of 15.28 m^2/g and a PZC at pH 3. Their size ranges from 37.36 to 71.33 nm, as indicated by TEM. They also exhibited an antioxidant activity of 85.57% at 250 μg/mL and an antibacterial activity with MIC and MBC values of 50 and 100 mg/mL, respectively, against both *E. coli* and *S. aureus*.

The best adsorption results for CIP removal by the green ZnO NPs were achieved at 125 mg/L initial concentration, 4 g/L dose, pH 5, and 25 °C after 60 min, yielding 86.77 ± 0.82% removal and 27.07 ± 0.26 mg/g adsorption capacity. As for TET, the highest adsorption capacity of 15.88 ± 0.37 mg/g was obtained at 125 mg/L initial concentration, while the highest % removal of 67.86 ± 3.41% was attained at 25 mg/L initial concentration, both using a 4 g/L dose at pH 5 and 25 °C after 120 min. The green ZnO NPs achieved 79.71% ± 0.28 and 61.55% ± 0.53 simultaneous removal of 10 mg/L CIP and 25 mg/L TET, respectively, in a binary tap water system, indicating their successful utilization in a wastewater simulation system. The adsorption of both CIP and TET by the green ZnO NPs was best described by the Langmuir isotherm and pseudo-second-order kinetics. The binding mechanism is likely to be electrostatic, possibly accompanied by hydrogen bonding and van der Waals. CIP was bound to the nanoparticles more strongly than TET, as supported by the values of the Langmuir association constants, due to its higher charge and smaller size. The regeneration and reuse of the adsorbent were possible for 5 cycles, with a loss in performance as the cycles progressed. The adsorptive performance of the green ZnO NPs was also compared to that of commercial ZnO NPs and found to be superior or comparable at the investigated concentrations for both CIP and TET. Last, factorial design revealed that initial concentration, adsorbent

dose, and time affect both % removal and adsorption capacity. The present study covers a wide range of contaminant concentrations from 10 to 100 mg/mL that are more relevant to industrial wastewater matrices. For future work, the adsorption behavior of the green ZnO NPs in a real wastewater system could be examined in view of the promising findings obtained in single and binary tap water systems. To conclude, this work presents an innovative, competitive, and environmentally friendly approach for the adsorptive removal of CIP and TET from water.

■ ASSOCIATED CONTENT

ⓈI Supporting Information

The Supporting Information is available free of charge at https://pubs.acs.org/doi/10.1021/acsomega.3c09044.

> Scatter plot displaying the relation between independent and dependent variable, residuals versus fits plot, Q−Q plot, and histogram displaying distribution of the residuals of the model to test their variance and normality; interaction plots of different factors and their effect on the dependent variable and particle size; FTIR and XRD spectra of commercial ZnO NPs; EDX analysis of green ZnO NPs before adsorption and after CIP and TET adsorption; CIP speciation diagram; TET speciation diagram; scatter plot displaying influence of independent variables on the dependent variables q and % removal, and on each other for CIP adsorption; distribution of CIP adsorption data to test their error variance and normality using residuals versus fits plot, Q−Q plot and histogram for q and % removal; interaction plots of factors affecting CIP adsorption and their effect on log q and log % removal; scatter plot displaying influence of independent variables on dependent variables q and % removal and on each other for TET adsorption; distribution of TET adsorption data to test their error variance and normality using residuals versus fits plot, Q−Q plot, and histogram for q and % removal; interaction plots of factors for TET adsorption and their effect on log q and log % removal; CIP and TET adsorption isotherm modeling linear plots; pseudo-

first- and pseudo-second-order kinetic modeling linear plots for CIP and TET adsorption; Elovich kinetic modeling linear plots for CIP and TET adsorption; CIP and TET kinetic modeling parameters; and CIP and TET Elovich kinetic modeling parameters (PDF)

■ AUTHOR INFORMATION

Corresponding Author

    Mayyada M.H. El-Sayed − *Department of Chemistry, School of Sciences and Engineering, The American University in Cairo, New Cairo 11835 Cairo, Egypt;* ⊙ orcid.org/0000-0001-6257-5748; Email: Mayyada@aucegypt.edu

Authors

    Hania A. Guirguis − *Department of Chemistry, School of Sciences and Engineering, The American University in Cairo, New Cairo 11835 Cairo, Egypt*

    Noha Youssef − *Mathematics and Actuarial Science Department, School of Sciences and Engineering, The American University in Cairo, New Cairo 11835 Cairo, Egypt*

    Mariam William − *Department of Chemistry, School of Sciences and Engineering, The American University in Cairo, New Cairo 11835 Cairo, Egypt*

    Dania Abdel-Dayem − *Department of Chemistry, School of Sciences and Engineering, The American University in Cairo, New Cairo 11835 Cairo, Egypt*

Complete contact information is available at:
https://pubs.acs.org/10.1021/acsomega.3c09044

Author Contributions

Conceptualization; methodology, M.E., H.G., and D.A.; software, N.Y.; formal analysis, H.G., D.A., and M.W.; data curation, M.E., H.G., and N.Y.; writing—original draft preparation, H.G.; writing—review and editing, M.E. and N.Y.; supervision, M.E.

Notes

The authors declare no competing financial interest.

■ ACKNOWLEDGMENTS

■ REFERENCES

(1) Tortajada, C. Contributions of Recycled Wastewater to Clean Water and Sanitation Sustainable Development Goals. *npj Clean Water* **2020**, *3* (1), 22−26.

(2) Abou-Elela, S. I. Constructed Wetlands: The Green Technology for Municipal Wastewater Treatment and Reuse in Agriculture. In *Unconventional Water Resources and Agriculture in Egypt*; Negm, A. M., Ed.; Springer International Publishing, 2017; pp 189−240.

(3) Obaideen, K.; Shehata, N.; Taha, E.; Ali, M. The Role of Wastewater Treatment in Achieving Sustainable Development Goals (SDGs) and Sustainability Guideline. *Energy Nexus* **2022**, *7*, 100112.

(4) Rizzo, L.; Malato, S.; Antakyali, D.; Beretsou, V. G.; Đolić, M. B.; Gernjak, W.; Heath, E.; Ivancev-Tumbas, I.; Karaolia, P.; Lado Ribeiro, A. R.; Mascolo, G.; McArdell, C. S.; Schaar, H.; Silva, A. M. T.; Fatta-Kassinos, D. Consolidated vs New Advanced Treatment Methods for the Removal of Contaminants of Emerging Concern from Urban Wastewater. *Sci. Total Environ.* **2019**, *655*, 986−1008.

(5) Dewi, R.; Shamsuddin, N.; Bakar, M. S. A.; Santos, J. H.; Bilad, M. R.; Lim, L. H.; Tinggi, S.; Kesehatan, I.; Tunas, B. Progress in Emerging Contaminants Removal by Adsorption/Membrane Filtration-Based Technologies: A Review. *Indones. J. Sci. Technol.* **2021**, *6* (3), 577−618.

(6) United States Environmental Protection Agency. *Occurrence of Contaminants of Emerging Concern in Wastewater From Nine Publicly Owned Treatment Works*, 2009.

(7) Halden, R. U. Epistemology of Contaminants of Emerging Concern and Literature Meta-Analysis. *J. Hazard. Mater.* **2015**, *282*, 2−9.

(8) Raghav, M.; Eden, S.; Mitchell, K.; White, B. *Arroyo 2013 Contaminants of Emerging Concern in Water*, 2013.

(9) Magalhães-Ghiotto, G. A.; Oliveira, A. M. d.; Natal, J. P. S.; Bergamasco, R.; Gomes, R. G. Green Nanoparticles in Water Treatment: A Review of Research Trends, Applications, Environmental Aspects and Large-Scale Production. *Environ. Nanotechnology, Monit. Manag.* **2021**, *16* (June), 100526.

(10) Roma, M.; Weller, M.; Wentzell, S. *Removal of Ciprofloxacin from Water Using Adsorption, UV Photolysis and UV/H$_2$O$_2$ Degradation*; Worcester Polytechnic Institute, 2011.

(11) Kummerer, K. Pharmaceuticals in the Environment. *Annu. Rev. Environ. Resour.* **2010**, *35*, 57−75.

(12) Huang, F.; An, Z.; Moran, M. J.; Liu, F. Recognition of Typical Antibiotic Residues in Environmental Media Related to Groundwater in China (2009−2019). *J. Hazard. Mater.* **2020**, *399*, 122813.

(13) European Union. *Commission Implementing Decision (EU) 2018/840*; Official Journal of the European Union, 2018; pp 9−12.

(14) Petrie, B.; Barden, R.; Kasprzyk-Hordern, B. A Review on Emerging Contaminants in Wastewaters and the Environment: Current Knowledge, Understudied Areas and Recommendations for Future Monitoring. *Water Res.* **2015**, *72*, 3−27.

(15) Fares, M. M.; Al-Rub, F. A. A.; Mohammad, A. R. Ultimate Eradication of the Ciprofloxacin Antibiotic from the Ecosystem by Nanohybrid Go/o-Cnts. *ACS Omega* **2020**, *5* (9), 4457−4468.

(16) Lei, X.; Lu, J.; Liu, Z.; Tong, Y.; Li, S. Concentration and Distribution of Antibiotics in Water-Sediment System of Bosten Lake, Xinjiang. *Environ. Sci. Pollut. Res.* **2015**, *22*, 1670−1678.

(17) Rodriguez-Mozaz, S.; Vaz-Moreira, I.; Varela Della Giustina, S.; Llorca, M.; Barceló, D.; Schubert, S.; Berendonk, T. U.; Michael-Kordatou, I.; Fatta-Kassinos, D.; Martinez, J. L.; Elpers, C.; Henriques, I.; Jaeger, T.; Schwartz, T.; Paulshus, E.; O'Sullivan, K.; Pärnänen, K. M.; Virta, M.; Do, T. T.; Walsh, F.; Manaia, C. M. Antibiotic Residues in Final Effluents of European Wastewater Treatment Plants and Their Impact on the Aquatic Environment. *Environ. Int.* **2020**, *140*, 105733.

(18) Mutiyar, P. K.; Mittal, A. K. Risk Assessment of Antibiotic Residues in Different Water Matrices in India: Key Issues and Challenges. *Environ. Sci. Pollut. Res.* **2014**, *21*, 7723−7736.

(19) He, K.; Blaney, L. Systematic Optimization of an SPE with HPLC-FLD Method for Fluoroquinolone Detection in Wastewater. *J. Hazard. Mater.* **2015**, *282*, 96−105.

(20) Borghi, A. A.; Palma, M. S. A. Tetracycline: Production, Waste Treatment and Environmental Impact Assessment. *Brazilian J. Pharm. Sci.* **2014**, *50* (1), 25−40.

(21) Adesoji, A. T.; Ogunjobi, A. A.; Olatoye, I. O.; Douglas, D. R. Prevalence of Tetracycline Resistance Genes among Multi-Drug Resistant Bacteria from Selected Water Distribution Systems in Southwestern Nigeria. *Ann. Clin. Microbiol. Antimicrob.* **2015**, *14* (1), 35−38.

(22) Gopal, G.; Alex, S. A.; Chandrasekaran, N.; Mukherjee, A. A Review on Tetracycline Removal from Aqueous Systems by Advanced Treatment Techniques. *RSC Adv.* **2020**, *10* (45), 27081−27095.

(23) Amangelsin, Y.; Semenova, Y.; Dadar, M.; Aljofan, M.; Bjørklund, G. The Impact of Tetracycline Pollution on the Aquatic Environment and Removal Strategies. *Antibiotics* **2023**, *12* (3), 440−515.

(24) Milić, N.; Milanović, M.; Letić, N. G.; Sekulić, M. T.; Radonić, J.; Mihajlović, I.; Miloradov, M. V. Occurrence of Antibiotics as Emerging Contaminant Substances in Aquatic Environment. *Int. J. Environ. Health Res.* 2013, 23 (4), 296−310.

(25) Karthikeyan, K. G.; Meyer, M. T. Occurrence of Antibiotics in Wastewater Treatment Facilities in Wisconsin, USA. *Sci. Total Environ.* 2006, 361 (1−3), 196−207.

(26) Batt, A. L.; Kim, S.; Aga, D. S. Comparison of the Occurrence of Antibiotics in Four Full-Scale Wastewater Treatment Plants with Varying Designs and Operations. *Chemosphere* 2007, 68 (3), 428−435.

(27) Patel, M.; Kumar, R.; Kishor, K.; Mlsna, T.; Pittman, C. U.; Mohan, D. Pharmaceuticals of Emerging Concern in Aquatic Systems: Chemistry, Occurrence, Effects, and Removal Methods. *Chem. Rev.* 2019, 119 (6), 3510−3673.

(28) Adeleye, A. S.; Conway, J. R.; Garner, K.; Huang, Y.; Su, Y.; Keller, A. A. Engineered Nanomaterials for Water Treatment and Remediation: Costs, Benefits, and Applicability. *Chem. Eng. J.* 2016, 286, 640−662.

(29) Harrabi, M.; Varela Della Giustina, S.; Aloulou, F.; Rodriguez-Mozaz, S.; Barcelo, D.; Elleuch, B. Analysis of multiclass antibiotic residues in urban wastewater in Tunisia. *Environ. Nanotechnology, Monit. Manag.* 2018, 10, 163−170.

(30) Kermia, A. E. B.; Fouial-Djebbar, D.; Mohamed Trar, M. Occurrence, Fate and Removal Efficiencies of Pharmaceuticals in Wastewater Treatment Plants (WWTPs) Discharging in the Coastal Environment of Algiers. *Comptes Rendus Chim.* 2016, 19 (8), 963.

(31) Al Qarni, H.; Collier, P.; O'Keeffe, J.; Akunna, J. Investigating the removal of some pharmaceutical compounds in hospital wastewater treatment plants operating in Saudi Arabia. *Environ. Sci. Pollut. Res.* 2016, 23 (13), 13003−13014.

(32) Khalafi, T.; Buazar, F.; Ghanemi, K. Phycosynthesis and Enhanced Photocatalytic Activity of Zinc Oxide Nanoparticles Toward Organosulfur Pollutants. *Sci. Rep.* 2019, 9 (1), 6866−6910.

(33) Genç, N.; Dogan, E. C. Adsorption Kinetics of the Antibiotic Ciprofloxacin on Bentonite, Activated Carbon, Zeolite, and Pumice. *Desalin. Water Treat.* 2015, 53 (3), 785−793.

(34) Liu, M. K.; Liu, Y. Y.; Bao, D. D.; Zhu, G.; Yang, G. H.; Geng, J. F.; Li, H. T. Effective Removal of Tetracycline Antibiotics from Water Using Hybrid Carbon Membranes. *Sci. Rep.* 2017, 7, 43717−43718.

(35) Zhu, H.; Chen, T.; Liu, J.; Li, D. Adsorption of Tetracycline Antibiotics from an Aqueous Solution onto Graphene Oxide/Calcium Alginate Composite Fibers. *RSC Adv.* 2018, 8 (5), 2616−2621.

(36) Chang, J.; Shen, Z.; Hu, X.; Schulman, E.; Cui, C.; Guo, Q.; Tian, H. Adsorption of Tetracycline by Shrimp Shell Waste from Aqueous Solutions: Adsorption Isotherm, Kinetics Modeling and Mechanism. *ACS Omega* 2020, 5, 3467−3477.

(37) El-Shafey, E. S. I.; Al-Lawati, H.; Al-Sumri, A. S. Ciprofloxacin Adsorption from Aqueous Solution onto Chemically Prepared Carbon from Date Palm Leaflets. *J. Environ. Sci.* 2012, 24 (9), 1579−1586.

(38) Dhiman, N.; Sharma, N. Batch Adsorption Studies on the Removal of Ciprofloxacin Hydrochloride from Aqueous Solution Using ZnO Nanoparticles and Groundnut (Arachis Hypogaea) Shell Powder: A Comparison*. *Indian Chem. Eng.* 2019, 61 (1), 67−76.

(39) Peñafiel, M. E.; Vanegas, E.; Bermejo, D.; Matesanz, J. M.; Ormad, M. P. Organic Residues as Adsorbent for the Removal of Ciprofloxacin from Aqueous Solution. *Hyperfine Interact.* 2019, 240, 71.

(40) Najafpoor, A. A.; Nemati Sani, O.; Alidadi, H.; Yazdani, M.; Navaei Fezabady, A. A.; Taghavi, M. Optimization of Ciprofloxacin Adsorption from Synthetic Wastewaters Using γ-Al2O3 Nanoparticles: An Experimental Design Based on Response Surface Methodology. *Colloids Interface Sci. Commun.* 2019, 33, 100212.

(41) Sharma, N.; Dhiman, N. Kinetic and Thermodynamic Studies for Ciprofloxacin Hydrochloride Adsorption from Aqueous Solution on CuO Nanoparticles. *Int. J. ChemTech Res.* 2017, 10 (5), 98−106.

(42) Khoshnamvand, N.; Ahmadi, S.; Mostafapour, F. K. Kinetic and Isotherm Studies on Ciprofloxacin an Adsorption Using Magnesium Oxide Nanoparticles. *J. Appl. Pharm. Sci.* 2017, 7 (11), 79−83.

(43) Sousa, W. R. D. N.; Oliveira, A. R.; Cruz Filho, J. F.; Dantas, T. C. M.; Santos, A. G. D.; Caldeira, V. P. S.; Luz, G. E. Ciprofloxacin Adsorption on ZnO Supported on SBA-15. *Water. Air. Soil Pollut.* 2018, 229 (4), 125.

(44) Mohammed, A. A.; Al-Musawi, T. J.; Kareem, S. L.; Zarrabi, M.; Al-Ma'abreh, A. M. Simultaneous Adsorption of Tetracycline, Amoxicillin, and Ciprofloxacin by Pistachio Shell Powder Coated with Zinc Oxide Nanoparticles. *Arab. J. Chem.* 2020, 13 (3), 4629−4643.

(45) Aljeboree, A. M.; Alkaim, A. F. Removal of Antibiotic Tetracycline (TCs) from Aqueous Solutions by Using Titanium Dioxide (TiO2) Nanoparticles as an Alternative Material. *J. Phys. Conf. Ser.* 2019, 1294 (5), 052059.

(46) A Ibrahim, M.; Ali A Shaban, M.; Rashid Hasan, Y.; J M-Ridha, M.; A Hussein, H.; M Abed, K.; J Mohammed, S.; Muhamad, M. H.; Abu Hasan, H. Simultaneous Adsorption of Ternary Antibiotics (Levofloxacin, Meropenem, and Tetracycline) by SunFlower Husk Coated with Copper Oxide Nanoparticles. *J. Ecol. Eng.* 2022, 23 (6), 30−42.

(47) Pham, T. D.; Vu, T. N.; Nguyen, H. L.; Le, P. H. P.; Hoang, T. S. Adsorptive Removal of Antibiotic Ciprofloxacin from Aqueous Solution Using Protein-Modified Nanosilica. *Polymers* 2020, 12 (1), 57.

(48) Zahoor, M.; Ullah, A.; Alam, S.; Muhammad, M.; Hendroko Setyobudi, R.; Zekker, I.; Sohail, A. Novel Magnetite Nanocomposites (Fe3 O4/C) for Efficient Immobilization of Ciprofloxacin from Aqueous Solutions through Adsorption Pretreatment and Membrane Processes. *Water* 2022, 14 (5), 724−810.

(49) Vardhan Patel, R.; Yadav, A. Photocatalytic MIL101(Fe)/ZnO Chitosan Composites for Adsorptive Removal of Tetracycline Antibiotics from the Aqueous Stream. *J. Mol. Struct.* 2022, 1252, 132128.

(50) Kaushik, R.; Narayanan, P.; Vasudevan, V.; Muthukumaran, G.; Usha, A. Nutrient Composition of Cultivated Stevia Leaves and the Influence of Polyphenols and Plant Pigments on Sensory and Antioxidant Properties of Leaf Extracts. *J. Food Sci. Technol.* 2010, 47 (1), 27−33.

(51) Chen, T. H.; Chen, S. C.; Chan, P.; Chu, Y. L.; Yang, H. Y.; Cheng, J. T. Mechanism of the Hypoglycemic Effect of Stevioside, a Glycoside of Stevia Rebaudiana. *Planta Med.* 2005, 71 (2), 108−113.

(52) Gasmalla, M. A. A.; Yang, R.; Hua, X. Stevia Rebaudiana Bertoni: An Alternative Sugar Replacer and Its Application in Food Industry. *Food Eng. Rev.* 2014, 6 (4), 150−162.

(53) Laguta, I.; Stavinskaya, O.; Kazakova, O.; Fesenko, T.; Brychka, S. Green Synthesis of Silver Nanoparticles Using Stevia Leaves Extracts. *Appl. Nanosci.* 2019, 9, 755−765.

(54) Varshneya, R.; Bhadauriaa, S.; SGaur, M. Biogenic Synthesis of Silver Nanocubes and Nanorods Using Sundried Stevia Rebaudiana Leaves. *Adv. Mater. Lett.* 2010, 1 (3), 232−237.

(55) Sadeghi, B.; Mohammadzadeh, M.; Babakhani, B. Green Synthesis of Gold Nanoparticles Using Stevia Rebaudiana Leaf Extracts: Characterization and Their Stability. *J. Photochem. Photobiol., B* 2015, 148, 101−106.

(56) Alijani, H. Q.; Pourseyedi, S.; Torkzadeh Mahani, M.; Khatami, M. Green Synthesis of Zinc Sulfide (ZnS) Nanoparticles Using Stevia Rebaudiana Bertoni and Evaluation of Its Cytotoxic Properties. *J. Mol. Struct.* 2019, 1175, 214−218.

(57) Khatami, M.; Alijani, H. Q.; Heli, H.; Sharifi, I. Rectangular Shaped Zinc Oxide Nanoparticles: Green Synthesis by Stevia and Its Biomedical Efficiency. *Ceram. Int.* 2018, 44 (13), 15596−15602.

(58) Essa, H. L.; Abdelfattah, M. S.; Marzouk, A. S.; Guirguis, H. A.; El-Sayed, M. M. H. Nano-Formulations of Copper Species Coated with Sulfated Polysaccharide Extracts and Assessment of Their Phytotoxicity on Wheat (Triticum Aestivum L.) Seedlings in Seed Germination, Foliar and Soil Applications. *Appl. Sci.* 2020, 10 (18), 6302.

(59) Abdol Aziz, R. A.; Bronny, B. G. A. Zinc Oxide Nanoparticle Synthesis With Banana Peel Extract From Jackfruit Banana: Effects of Temperature. *Int. J. Technol. Res. Eng.* **2019**, 26−40.

(60) Albalasmeh, A. A.; Berhe, A. A.; Ghezzehei, T. A. A New Method for Rapid Determination of Carbohydrate and Total Carbon Concentrations Using UV Spectrophotometry. *Carbohydr. Polym.* **2013**, *97* (2), 253−261.

(61) El-Sayed, M.; Fleita, D.; Rifaat, D.; Essa, H. Developments in the Extraction of Antioxidants From Marine Algal Species. *Ingredients Extraction by Physico-Chemical Methods in Food*; Elsevier Inc., 2017; pp 367−397..

(62) Mishra, K.; Ojha, H.; Chaudhury, N. K. Estimation of Antiradical Properties of Antioxidants Using DPPH Assay: A Critical Review and Results. *Food Chem.* **2012**, *130* (4), 1036−1043.

(63) Happy, A.; Soumya, M.; Venkat Kumar, S.; Rajeshkumar, S.; Sheba, R. D.; Lakshmi, T.; Deepak Nallaswamy, V. Phyto-Assisted Synthesis of Zinc Oxide Nanoparticles Using Cassia Alata and Its Antibacterial Activity against Escherichia Coli. *Biochem. Biophys. Reports* **2019**, *17*, 208−211.

(64) Azizi, S.; Shahri, M. M.; Mohamad, R. Green Synthesis of Zinc Oxide Nanoparticles for Enhanced Adsorption of Lead Ions from Aqueous Solutions: Equilibrium, Kinetic and Thermodynamic Studies. *Molecules* **2017**, *22* (6), 831.

(65) Zheng, Y.; Fu, L.; Han, F.; Wang, A.; Cai, W.; Yu, J.; Yang, J.; Peng, F. Green Biosynthesis and Characterization of Zinc Oxide Nanoparticles Using Corymbia Citriodora Leaf Extract and Their Photocatalytic Activity. *Green Chem. Lett. Rev.* **2015**, *8* (2), 59−63.

(66) Martono, Y.; Rondonuwu, F. S.; Trihandaru, S. Classification of Stevia Rebaudiana Using Near Infrared Spectroscopy and Multivariate Data Analysis. *Mater. Sci. Forum* **2017**, *901*, 103−109.

(67) Yilmaz, M.; Turkdemir, H.; Kilic, M. A.; Bayram, E.; Cicek, A.; Mete, A.; Ulug, B. Biosynthesis of Silver Nanoparticles Using Leaves of Stevia Rebaudiana. *Mater. Chem. Phys.* **2011**, *130* (3), 1195−1202.

(68) Essa, H.; Guirguis, H.; El-Sayed, M.; Rifaat, D.; Abdelfattah, M. Ultrasonically-Extracted Marine Polysaccharides as Potential Green Antioxidant Alternatives. *Proceedings* **2020**, 7606.

(69) Naziruddin, M. A.; Kian, L. K.; Jawaid, M.; Fouad, H.; Sanny, M.; Braganca, R. M. Sage Biomass Powders by Supercritical Fluid Extraction and Hydro-Distillation Techniques: A Comparative Study of Biological and Chemical Properties. *Biomass Convers. Biorefinery* **2021**, *13*, 13091−13101.

(70) Saleh, S. S.; El-shayeb, N. S. A. Impact of Spirulina Platensis and Stevia Rebaudiana on Growth and Essential Oil Production of Basil Ocimum Citriodorum. *J. Agric. Rural Res.* **2020**, *3* (2), 36−45.

(71) Bala, N.; Saha, S.; Chakraborty, M.; Maiti, M.; Das, S.; Basu, R.; Nandy, P. Green Synthesis of Zinc Oxide Nanoparticles Using Hibiscus Subdariffa Leaf Extract: Effect of Temperature on Synthesis, Anti-Bacterial Activity and Anti-Diabetic Activity. *RSC Adv.* **2015**, *5* (7), 4993−5003.

(72) Soren, S.; Kumar, S.; Mishra, S.; Jena, P. K.; Verma, S. K.; Parhi, P. Evaluation of antibacterial and antioxidant potential of the zinc oxide nanoparticles synthesized by aqueous and polyol method. *Microb. Pthogenes.* **2018**, *119*, 145−151.

(73) Lowell, S.; Shields, J. E.; Thomas, M. A.; Thommes, M. *Characterization of Porous Solids and Powders: Surface Area, Pore Size and Density*; Springer Science + Business Media: New York, 2004..

(74) Safawo, T.; Sandeep, B. V.; Pola, S.; Tadesse, A. Synthesis and Characterization of Zinc Oxide Nanoparticles Using Tuber Extract of Anchote (Coccinia Abyssinica (Lam.) Cong.) for Antimicrobial and Antioxidant Activity Assessment. *OpenNano* **2018**, *3* (May), 56−63.

(75) Sánchez-Rangel, J. C.; Benavides, J.; Heredia, J. B.; Cisneros-Zevallos, L.; Jacobo-Velázquez, D. A. The Folin-Ciocalteu Assay Revisited: Improvement of Its Specificity for Total Phenolic Content Determination. *Anal. Methods* **2013**, *5* (21), 5990−5999.

(76) Lamuela-Raventós, R. M. Folin-Ciocalteu Method for the Measurement of Total Phenolic Content and Antioxidant Capacity. In *Measurement of Antioxidant Activity and Capacity: Recent Trends and Applications*; Apak, R., Capanoglu, E., Shahidi, F., Eds.; John Wiley & Sonns Ltd., 2018; pp 107−115..

(77) Shkal, K. E. M.; Azab, A. E.; Attia, A. M. Zinc Oxide Nanoparticles Attenuate the Oxidative Damage and Disturbance in Antioxidant Defense System Induced by Cyclophosphamide in Male Albino Rats. *Insights Biol.* **2020**, *4*, 1−8.

(78) Elkady, M. F.; Shokry Hassan, H.; Hafez, E. E.; Fouad, A. Construction of Zinc Oxide into Different Morphological Structures to Be Utilized as Antimicrobial Agent against Multidrug Resistant Bacteria. *Bioinorg. Chem. Appl.* **2015**, *2015*, 1−20.

(79) Dimapilis, E. A. S.; Hsu, C. S.; Mendoza, R. M. O.; Lu, M. C. Zinc Oxide Nanoparticles for Water Disinfection. *Sustain. Environ. Res.* **2018**, *28* (2), 47−56.

(80) Mohammed, A. A.; Kareem, S. L. Adsorption of Tetracycline Fom Wastewater by Using Pistachio Shell Coated with ZnO Nanoparticles: Equilibrium, Kinetic and Isotherm Studies. *Alexandria Eng. J.* **2019**, *58* (3), 917−928.

(81) Atkins, P.; De Paula, J. *Atkins' Physical Chemistry*, 9th ed.; Oxford University Press: Oxford, 2010.

(82) Ahile, U. J.; Adejo, S. O.; Ubwa, S. T.; Iorhuna, T. B.; Tyohemba, R. L.; Ikyagh, M. G.; Utange, P. I. Kinetics and Adsorption Studies of Tetracycline from Aqueous Solution Using Melon Husk. *IOSR J. Appl. Chem.* **2018**, *11* (2), 26−35.

(83) Guler, U. A.; Sarioglu, M. Removal of Tetracycline from Wastewater Using Pumice Stone: Equilibrium, Kinetic and Thermodynamic Studies. *J. Environ. Heal. Sci. Eng.* **2014**, *12* (1), 79.

(84) Khalaf, S. M.; Al-Mahmoud, S. M. Adsorption of Tetracycline Antibiotic from Aqueous Solutions Using Natural Iraqi Bentonite. *Egypt. J. Chem.* **2021**, *64* (10), 5511−5519.

(85) Hamoudi, S. A.; Hamdi, B.; Brendlé, J. Tetracycline Removal from Water by Adsorption on Geomaterial, Activated Carbon and Clay Adsorbents. *Ecol. Chem. Eng. S* **2021**, *28* (3), 303−328.

(86) Al-Musawi, T. J.; Mahvi, A. H.; Khatibi, A. D.; Balarak, D. Effective Adsorption of Ciprofloxacin Antibiotic Using Powdered Activated Carbon Magnetized by Iron(III) Oxide Magnetic Nano-particles. *J. Porous Mater.* **2021**, *28* (3), 835−852.

(87) Bao, J.; Zhu, Y.; Yuan, S.; Wang, F.; Tang, H.; Bao, Z.; Zhou, H.; Chen, Y. Adsorption of Tetracycline with Reduced Graphene Oxide Decorated with MnFe2O4 Nanoparticles. *Nanoscale Res. Lett.* **2018**, *13*, 396.

(88) Lin, C. C.; Lee, C. Y. Adsorption of Ciprofloxacin in Water Using Fe3O4 Nanoparticles Formed at Low Temperature and High Reactant Concentrations in a Rotating Packed Bed with Co-Precipitation. *Mater. Chem. Phys.* **2020**, *240*, 122049.